

A Statically Condensed Discontinuous Galerkin Spectral Element Method on Gauss-Lobatto Nodes for the Compressible Navier-Stokes Equations

Andrés M. Rueda-Ramírez^{a,b,*}, Esteban Ferrer^{a,b}, David A. Kopriva^c, Gonzalo Rubio^{a,b}, Eusebio Valero^{a,b}

^a*ETSIAE-UPM (School of Aeronautics - Universidad Politécnica de Madrid) , Plaza de Cardenal Cisneros 3, 28040 Madrid, Spain.*

^b*Center for Computational Simulation, Universidad Politécnica de Madrid, Campus de Montegancedo, Boadilla del Monte, 28660 Madrid, Spain.*

^c*Department of Mathematics, Florida State University and Computational Science Research Center, San Diego State University.*

Abstract

In this paper, we present a static-condensation method for time-implicit discretizations of the Discontinuous Galerkin Spectral Element Method on Gauss-Lobatto points (GL-DGSEM). We show that it is possible to reorganize the linear system that results from the implicit time-integration of the GL-DGSEM as a Schur complement problem, which can be efficiently solved using static condensation. The use of static condensation reduces the linear system size and improves the conditioning of the system matrix, which translates into shorter computational times.

The statically condensed GL-DGSEM presented here can be applied to any set of linear or nonlinear advection-diffusion partial differential equations in conservation form. We test it to solve the compressible Navier-Stokes equations with direct and Krylov subspace solvers, and we show for a selected problem that using the statically condensed GL-DGSEM leads to speed-ups of up to 140 when compared to the time-explicit GL-DGSEM, and speed-ups of up to 2.5 when compared with the time-implicit GL-DGSEM that solves the global system.

The GL-DGSEM has gained increasing popularity in recent years because it satisfies the summation-by-parts property, which enables the construction of provably entropy stable schemes, and because it is computationally cheaper and easier to implement than most other high-order Discontinuous Galerkin (DG) methods. In this paper, we show that the GL-DGSEM has an additional advantage: It can be statically condensed.

Keywords: High-order discontinuous Galerkin, Implicit time-integration, Static condensation.

Contents

1	Introduction	2
2	Mathematical Background	4
2.1	Notation	4
2.2	The Discontinuous Galerkin Spectral Element Method (DGSEM)	5
2.3	Time-Implicit DGSEM	8
2.3.1	Advective Terms	8
2.3.2	Diffusive Terms	9
2.4	Static Condensation	10

*Corresponding authors:

Email address: am.rueda@upm.es (Andrés M. Rueda-Ramírez)

2.4.1	Continuous Galerkin Methods	11
2.4.2	Discontinuous Galerkin Methods	12
3	Statically Condensed GL-DGSEM	13
3.1	Jacobian Sparsity Patterns	13
3.1.1	Advective Terms	13
3.1.2	Diffusive Terms	15
3.2	Analysis and Implementation	16
4	Numerical Example	19
5	Final Remarks	23

1. Introduction

High-order Discontinuous Galerkin (DG) methods have become popular to solve linear and nonlinear Partial Differential Equations (PDEs) because of their high accuracy and flexibility [1–3]. These methods rely on a variational formulation where the continuity constraint on element interfaces is relaxed, allowing for discontinuities in the numerical solution. This feature makes DG methods very robust for solving advection dominated problems, such as the ones encountered in fluid dynamics applications.

In spite of the increased popularity of high-order methods, most of the production-quality CFD codes in use are still low order: e.g. in the aerospace industry [4–6], in weather prediction [7], in astrophysics [8, 9], etc. A likely reason is that the long years of development on low-order methods have produced very computational-cost-effective solvers that are difficult to compete against. In this work, we seek to reduce the cost of computing high-order accurate solutions of the Navier-Stokes equations by choosing a computationally efficient DG method, doing implicit time-integration and using static condensation.

The variational formulation of DG methods requires the evaluation of volume and surface integrals. These integrals are usually approximated with a quadrature rule, which uses the value of the integrated functions on nodes with specific positions.

In this paper, we use the Discontinuous Galerkin Spectral Element Method (DGSEM), as it is one of the most computationally efficient high-order DG schemes available [10]. The DGSEM is usually called a collocation method since it stores the solution variables at the nodes of the quadrature rule and reconstructs the solution using discretely orthogonal basis functions. The collocation property gives the DGSEM a computational advantage over other modal and nodal DG methods, where the conservative variables and the fluxes must be evaluated on the quadrature nodes as an additional step. Moreover, the use of a collocated quadrature and orthogonal bases equips the DGSEM with a diagonal mass matrix and relatively cheap-to-compute operators.

The standard choices for the position of the nodes of the DGSEM are the Gauss and the Gauss-Lobatto quadrature points. Several advantages have been identified for the DGSEM on Gauss-Lobatto nodes (the GL-DGSEM) over the one that uses Gauss nodes (the G-DGSEM). The first advantage is that, in the former method, the solution is stored where it is needed for the evaluation of the surface integrals, whereas it is not in the G-DGSEM. This makes the GL-DGSEM computationally cheaper and easier to implement since the solution does not have to be interpolated to the element boundaries, as in the G-DGSEM. In addition, it has been shown that the GL-DGSEM allows taking larger time steps than the G-DGSEM because of the inherent spectrum of the spatial operator [11]. Furthermore, the GL-DGSEM can be used to unify certain diffusive numerical fluxes as it has been shown that the Bassi-Rebay 1 scheme is a special case of the symmetric Interior Penalty method when Gauss-Lobatto nodes are used [12].

The only disadvantage of the Gauss-Lobatto quadrature is that it is not as accurate as the Gauss quadrature: The numerical integration is only exact for polynomials of order up to $2N - 1$ when using a Gauss-Lobatto quadrature with $N + 1$ nodes, whereas it is exact for polynomials of order up to $2N + 1$ when using a Gauss quadrature with the same number of nodes [13]. An inexact evaluation of the integrals induces aliasing errors that can trigger instabilities, which in turn can make the solution blow up, specially at high

Reynolds numbers [14]. The traditional DGSEM on Gauss nodes also suffers from those instabilities, but they appear *sooner* when Gauss-Lobatto nodes are used [11, 14].

The common solution to aliasing-driven instabilities is to increase the number of quadrature points to reduce (or eliminate) the aliasing errors, in an approach that is called polynomial dealiasing or over-integration. The over-integration strategy increases the computational cost since collocation is no longer possible. Moreover, an exact numerical integration is not always achievable, no matter the number of quadrature points. For some systems of equations, like the compressible Euler or Navier-Stokes, the fluxes are not polynomials, but ratios of polynomials [15].

It has been shown that the aliasing driven instabilities can be eliminated with the use of an entropy stable split form of the governing equations [16, 17]. This can be achieved while keeping discrete conservation properties if the discretization scheme satisfies the summation-by-parts simultaneous-approximation-term (SBP-SAT) property [17]. Moreover, Gassner [18] showed that the GL-DGSEM satisfies the SBP-SAT property. As a result, entropy stable split forms can be formulated for the GL-DGSEM, e.g. for the Burgers equation [18], the compressible Navier-Stokes equations [15], the MHD equations [19], the Cahn-Hilliard equation [20], the incompressible Navier-Stokes equations [21], etc. The split form has a dealiasing effect that makes the GL-DGSEM provably stable (something that is not achievable with simple polynomial dealiasing), while still being computationally cheaper than over-integrated methods and yielding comparable results [22]. All these studies point out that the GL-DGSEM has a numerical superiority over the traditional G-DGSEM.

The authors note that in a recent publication, Chan et al. [23] proved that entropy-stable DGSEM discretizations can also be obtained using Gauss nodes. However, this recent technology requires $12(N+1)^3$ extra flux evaluations, which renders it more expensive than the GL-DGSEM.

Static condensation [24] is a technique to reduce the size of linear systems. It has been widely used in the continuous Galerkin (CG) community to solve time-implicit discretizations [25–27]. However, because of the way the degrees of freedom of different elements are coupled in DG discretizations, static condensation is not directly applicable to general DG methods in an efficient manner.

To the author’s knowledge, two techniques have been developed to efficiently apply static condensation to DG schemes. The first technique was developed by Sherwin et al. [28], and uses specially tailored basis functions with which it is possible to statically condense the linear system that arises from the time-implicit DG discretization. Unfortunately, the new basis functions are neither orthogonal nor tensor-product expansions. Therefore, some properties are lost, like the existence of diagonal mass matrices [13], Kronecker multiplication matrices, the ability to perform anisotropic p -adaptation [41], among others.

The second technique is the hybridizable DG (or HDG) method, which was developed by Carrero and Cockburn [29, 30]. This method expands the linear system to include the numerical trace of the solution as new unknown, to statically condense it around this new variable. This technique has been proved to be computationally efficient [31, 32], but it imposes certain constraints on the numerical fluxes of the DG method, such as the need for the elliptic fluxes to be adjoint consistent and compact [30], and the requirement for the numerical fluxes of nonlinear advection-diffusion equations to have a specific mathematical form [31, 32]. As a result, not all the known Riemann solvers can be classified as suitable for HDG.

In this paper, we show that static condensation can be directly applied to the time-implicit GL-DGSEM in an efficient manner without the strong constraints that other statically condensed DG schemes have. Namely, we keep tensor-product orthogonal bases in a method that can be used with any choice of the numerical flux functions, with the only requirement for the viscous numerical flux one to be compact. We show, by means of a numerical experiment, that the method developed here provides speed-ups when compared to the time-explicit GL-DGSEM and the not statically condensed time-implicit GL-DGSEM. Therefore, this investigation reveals a further advantage of Gauss-Lobatto quadratures over traditional Gauss quadratures in the DGSEM. The method here exposed is a novel contribution, as it is not an HDG method and, to the authors’ knowledge, it has not been attempted before.

The paper is organized as follows. Section 2 provides the mathematical background that is needed for the derivations of this work. We briefly describe the DGSEM in Section 2.2, detail how to obtain time-

implicit DGSEM discretizations in Section 2.3, and provide an overview of the static-condensation method in Section 2.4. In Section 3, we analyze the sparsity patterns of DGSEM methods and demonstrate that static condensation can be efficiently applied when Gauss-Lobatto nodes are used. Next, we detail the implementation of the statically condensed GL-DGSEM that is used in this work. Finally, the method is tested for solving the compressible Navier-Stokes equations in Section 4.

2. Mathematical Background

2.1. Notation

We adopt the notation in [19, 33] to work with vectors of different nature. Spatial vectors are noted with an arrow on top (e.g. $\vec{x} = (x, y, z) \in \mathbb{R}^3$), state vectors are noted in bold (e.g. $\mathbf{q} = (\rho, \rho\vec{v}, \rho E)^T$), and block vectors, which contain a state vector in every spatial direction, are noted as

$$\vec{\mathbf{f}} = \begin{bmatrix} \mathbf{f}_1 \\ \mathbf{f}_2 \\ \mathbf{f}_3 \end{bmatrix} = \mathbf{f}_1 \hat{i} + \mathbf{f}_2 \hat{j} + \mathbf{f}_3 \hat{k}. \quad (1)$$

Moreover, we note generic vectors with a bold uppercase letter. For instance, a vector that contains the state variables in all degrees of freedom is noted as $\mathbf{Q} = [\mathbf{q}_1, \mathbf{q}_2, \dots, \mathbf{q}_{\text{NDOF}}]^T$, where NDOF is the number of degrees of freedom.

The gradient of a state vector is a block vector:

$$\vec{\nabla} \mathbf{q} = \begin{bmatrix} \partial_x \mathbf{q} \\ \partial_y \mathbf{q} \\ \partial_z \mathbf{q} \end{bmatrix} = \partial_x \mathbf{q} \hat{i} + \partial_y \mathbf{q} \hat{j} + \partial_z \mathbf{q} \hat{k}, \quad (2)$$

and the gradient of a spatial vector can be represented as a second order tensor, which can be written in matrix form using the outer product as

$$\underline{\mathbf{L}} = \vec{\nabla} \vec{v} = (\vec{\nabla} \otimes \vec{v})^T = (\vec{\nabla} \vec{v}^T)^T = \begin{bmatrix} \frac{\partial v_1}{\partial x} & \frac{\partial v_1}{\partial y} & \frac{\partial v_1}{\partial z} \\ \frac{\partial v_2}{\partial x} & \frac{\partial v_2}{\partial y} & \frac{\partial v_2}{\partial z} \\ \frac{\partial v_3}{\partial x} & \frac{\partial v_3}{\partial y} & \frac{\partial v_3}{\partial z} \end{bmatrix}. \quad (3)$$

The underline is used throughout this work for second order tensors and matrices.

Third order tensors are noted with a double underline, e.g. the flux derivative with respect to \mathbf{q} can be expressed as

$$\frac{\partial \vec{\mathbf{f}}}{\partial \mathbf{q}} = \underline{\underline{\mathbf{J}}} = \begin{bmatrix} \mathbf{J}_1 \\ \mathbf{J}_2 \\ \mathbf{J}_3 \end{bmatrix} = \begin{bmatrix} \frac{\partial \mathbf{f}_1}{\partial \mathbf{q}} \\ \frac{\partial \mathbf{f}_2}{\partial \mathbf{q}} \\ \frac{\partial \mathbf{f}_3}{\partial \mathbf{q}} \end{bmatrix}. \quad (4)$$

Similarly, fourth order tensors are noted with a triple underline. For example, the derivative of the flux with respect to $\vec{\nabla} \mathbf{q}$ can be written as

$$\frac{\partial \vec{\mathbf{f}}}{\partial (\vec{\nabla} \mathbf{q})} = \underline{\underline{\underline{\mathbf{G}}}} = \begin{bmatrix} \underline{\underline{\mathbf{G}}}_1 \\ \underline{\underline{\mathbf{G}}}_2 \\ \underline{\underline{\mathbf{G}}}_3 \end{bmatrix} = \begin{bmatrix} \frac{\partial \mathbf{f}_1}{\partial (\vec{\nabla} \mathbf{q})} \\ \frac{\partial \mathbf{f}_2}{\partial (\vec{\nabla} \mathbf{q})} \\ \frac{\partial \mathbf{f}_3}{\partial (\vec{\nabla} \mathbf{q})} \end{bmatrix} = \begin{bmatrix} \frac{\partial \mathbf{f}_1}{\partial (\partial_x \mathbf{q})} & \frac{\partial \mathbf{f}_1}{\partial (\partial_y \mathbf{q})} & \frac{\partial \mathbf{f}_1}{\partial (\partial_z \mathbf{q})} \\ \frac{\partial \mathbf{f}_2}{\partial (\partial_x \mathbf{q})} & \frac{\partial \mathbf{f}_2}{\partial (\partial_y \mathbf{q})} & \frac{\partial \mathbf{f}_2}{\partial (\partial_z \mathbf{q})} \\ \frac{\partial \mathbf{f}_3}{\partial (\partial_x \mathbf{q})} & \frac{\partial \mathbf{f}_3}{\partial (\partial_y \mathbf{q})} & \frac{\partial \mathbf{f}_3}{\partial (\partial_z \mathbf{q})} \end{bmatrix} = \begin{bmatrix} \underline{\underline{\mathbf{G}}}_{11} & \underline{\underline{\mathbf{G}}}_{12} & \underline{\underline{\mathbf{G}}}_{13} \\ \underline{\underline{\mathbf{G}}}_{21} & \underline{\underline{\mathbf{G}}}_{22} & \underline{\underline{\mathbf{G}}}_{23} \\ \underline{\underline{\mathbf{G}}}_{31} & \underline{\underline{\mathbf{G}}}_{32} & \underline{\underline{\mathbf{G}}}_{33} \end{bmatrix}. \quad (5)$$

The dot (inner) product of two block vectors is a scalar,

$$\vec{\mathbf{f}} \cdot \vec{\mathbf{g}} = \sum_{i=1}^d \mathbf{f}_i \cdot \mathbf{g}_i = \sum_{i=1}^d \mathbf{f}_i^T \mathbf{g}_i. \quad (6)$$

Moreover, the dot product of a spatial vector with a block vector is a state vector,

$$\vec{v} \cdot \vec{\mathbf{f}} = \sum_{i=1}^d v_i \mathbf{f}_i, \quad \vec{\nabla} \cdot \vec{\mathbf{f}} = \sum_{i=1}^d \partial_i \mathbf{f}_i. \quad (7)$$

Finally, the product of a third order tensor by a state vector is a block vector,

$$\underline{\underline{\mathbf{J}}} \mathbf{q} = \begin{bmatrix} \underline{\mathbf{J}}_1 \\ \underline{\mathbf{J}}_2 \\ \underline{\mathbf{J}}_3 \end{bmatrix} \mathbf{q} = \begin{bmatrix} \underline{\mathbf{J}}_1 \mathbf{q} \\ \underline{\mathbf{J}}_2 \mathbf{q} \\ \underline{\mathbf{J}}_3 \mathbf{q} \end{bmatrix}, \quad (8)$$

and the product of a fourth order tensor of d columns by a block vector is also a block vector, for example,

$$\underline{\underline{\underline{\mathbf{G}}}} \vec{\mathbf{g}} = \underline{\underline{\underline{\mathbf{G}}}} \vec{\nabla} \mathbf{q} = \begin{bmatrix} \underline{\underline{\mathbf{G}}}_{11} & \underline{\underline{\mathbf{G}}}_{12} & \underline{\underline{\mathbf{G}}}_{13} \\ \underline{\underline{\mathbf{G}}}_{21} & \underline{\underline{\mathbf{G}}}_{22} & \underline{\underline{\mathbf{G}}}_{23} \\ \underline{\underline{\mathbf{G}}}_{31} & \underline{\underline{\mathbf{G}}}_{32} & \underline{\underline{\mathbf{G}}}_{33} \end{bmatrix} \begin{bmatrix} \mathbf{g}_1 \\ \mathbf{g}_2 \\ \mathbf{g}_3 \end{bmatrix} = \begin{bmatrix} \underline{\underline{\mathbf{G}}}_{11} \mathbf{g}_1 + \underline{\underline{\mathbf{G}}}_{12} \mathbf{g}_2 + \underline{\underline{\mathbf{G}}}_{13} \mathbf{g}_3 \\ \underline{\underline{\mathbf{G}}}_{21} \mathbf{g}_1 + \underline{\underline{\mathbf{G}}}_{22} \mathbf{g}_2 + \underline{\underline{\mathbf{G}}}_{23} \mathbf{g}_3 \\ \underline{\underline{\mathbf{G}}}_{31} \mathbf{g}_1 + \underline{\underline{\mathbf{G}}}_{32} \mathbf{g}_2 + \underline{\underline{\mathbf{G}}}_{33} \mathbf{g}_3 \end{bmatrix}. \quad (9)$$

2.2. The Discontinuous Galerkin Spectral Element Method (DGSEM)

We consider the approximation of systems of conservation laws,

$$\partial_t \mathbf{q} + \vec{\nabla} \cdot \vec{\mathbf{f}} = \mathbf{0}, \quad \text{in } \Omega, \quad (10)$$

subject to appropriate boundary conditions, where \mathbf{q} is the state vector of conserved variables, and $\vec{\mathbf{f}}$ is the flux block vector, which depends on \mathbf{q} . In an advection-diffusion conservation law, the flux vector can be written as

$$\vec{\mathbf{f}} = \vec{\mathbf{f}}^a(\mathbf{q}) - \vec{\mathbf{f}}^\nu(\mathbf{q}, \vec{\nabla} \mathbf{q}), \quad (11)$$

where $\vec{\mathbf{f}}^a$ is the advective flux and $\vec{\mathbf{f}}^\nu$ is the diffusive flux.

Because of the dependency of the diffusive flux on $\vec{\nabla} \mathbf{q}$, (10) is a second order PDE. Following Arnold et al. [34], (10) can be rewritten as a first-order system,

$$\begin{cases} \partial_t \mathbf{q} + \vec{\nabla} \cdot (\vec{\mathbf{f}}^a(\mathbf{q}) - \vec{\mathbf{f}}^\nu(\mathbf{q}, \vec{\mathbf{g}})) = \mathbf{0}, & \text{in } \Omega, \\ \vec{\nabla} \mathbf{q} = \vec{\mathbf{g}}, & \text{in } \Omega. \end{cases} \quad (12a)$$

$$(12b)$$

To obtain the DG discretization of the system (12), we start by multiplying (12a) by an arbitrary and smooth test function, \mathbf{v} , and integrating by parts over the domain, Ω ,

$$\int_{\Omega} \partial_t \mathbf{q} \cdot \mathbf{v} d\Omega - \int_{\Omega} \vec{\mathbf{f}} \cdot \vec{\nabla} \mathbf{v} d\Omega + \int_{\partial\Omega} (\vec{\mathbf{f}} \cdot \vec{n}) \cdot \mathbf{v} dS = \mathbf{0}, \quad (13)$$

where \vec{n} is the normal unit vector on the boundary $\partial\Omega$.

Let the domain Ω be approximated by a tessellation $\mathcal{T} = \{e\}$, i.e. a combination of K spectral elements e of domain Ω^e and boundary $\partial\Omega^e$. Moreover, let \mathbf{q} , $\vec{\mathbf{f}}$ and \mathbf{v} be approximated by piece-wise polynomial functions \mathbf{q}^N , $\vec{\mathbf{f}}^N$ and \mathbf{v}^N (which are continuous in each element) defined in the space of L^2 functions

$$\mathcal{V}^N = \{\mathbf{v}^N \in L^2(\Omega) : \mathbf{v}^N|_{\Omega^e} \in \mathcal{P}^N(\Omega^e) \quad \forall \Omega^e \in \mathcal{T}\}, \quad (14)$$

where $\mathcal{P}^N(\Omega^e)$ is the space of polynomials of degree at most N defined in Ω^e , the domain of element e .

Since the functions in \mathcal{V}^N may be discontinuous at element interfaces, the quantity $\vec{\mathbf{f}}^N \cdot \vec{n}$ is not uniquely defined at the element traces. Therefore, it is replaced by a numerical flux function,

$$\vec{\mathbf{f}}^N \cdot \vec{n} \leftarrow \hat{\mathbf{f}} = \hat{\mathbf{f}}^a - \hat{\mathbf{f}}^\nu, \quad (15)$$

which allows one to uniquely define the flux at the element interfaces and to weakly prescribe the boundary data as a function of the normal vector and the state on both sides of the boundary/interface. Equation (13) can then be rewritten for each element as

$$\int_{\Omega^e} \partial_t \mathbf{q}^N \cdot \mathbf{v}^N d\Omega^e - \int_{\Omega^e} \vec{\mathbf{f}}^N \cdot \vec{\nabla} \mathbf{v}^N d\Omega^e + \int_{\partial\Omega^e} \hat{\mathbf{f}} \cdot \mathbf{v}^N dS^e = 0. \quad (16)$$

The quantities \mathbf{q}^N , \mathbf{v}^N and $\vec{\mathbf{f}}^N$ belong to the polynomial space \mathcal{V}^N . Therefore, it is possible to represent them inside every element as a linear combination of basis functions, $\phi_j \in \mathcal{P}^N(\Omega^e)$, so that

$$\mathbf{q}^N|_{\Omega^e} = \sum_{j=1}^{\text{NDOF}^e} \mathbf{q}_j^N \phi_j(\mathbf{x}), \quad \mathbf{v}^N|_{\Omega^e} = \sum_{j=1}^{\text{NDOF}^e} \mathbf{v}_j^N \phi_j(\mathbf{x}), \quad \vec{\mathbf{f}}^N|_{\Omega^e} = \sum_{j=1}^{\text{NDOF}^e} \vec{\mathbf{f}}_j^N \phi_j(\mathbf{x}), \quad (17)$$

where the (spatial) number of degrees of freedom (NDOF) in hexahedral elements depends on the polynomial order of the approximation, $\text{NDOF}^e = (N+1)^d$, where d is the number of spatial dimensions.

Since the test function \mathbf{v}^N is an arbitrary polynomial, (16) must hold for every basis function ϕ_j . Therefore, the DG discretization of (12a) becomes

$$\int_{\Omega^e} \partial_t \mathbf{q}^N \phi_j d\Omega^e - \int_{\Omega^e} \vec{\mathbf{f}}^N \cdot \vec{\nabla} \phi_j d\Omega^e + \int_{\partial\Omega^e} \hat{\mathbf{f}} \phi_j dS^e = 0, \quad (18)$$

Following a similar procedure, we can obtain the DG discretization of (12b) as

$$\int_{\Omega^e} \vec{\mathbf{g}}^N \phi_j d\Omega^e = - \int_{\Omega^e} \mathbf{q}^N \vec{\nabla} \phi_j d\Omega^e + \int_{\partial\Omega^e} \phi_j \hat{\mathbf{q}} \vec{n} dS^e \quad (19)$$

where $\hat{\mathbf{q}}$ is a numerical *flux* (actually the numerical trace of the solution) that corresponds to the interface value assumed by the state vector \mathbf{q} . Note that in the notation used here, the definition of the numerical trace of \mathbf{q} does not include the action of the normal vector.

The advective numerical flux, $\hat{\mathbf{f}}^a(\mathbf{q}^+, \mathbf{q}^-, \vec{n})$, is a function of the normal vector to the surface $\partial\Omega^e$, \vec{n} , of the discrete solution on element e ,

$$\mathbf{q}^+ = \sum_{j=1}^{\text{NDOF}^e} \mathbf{q}_j^N \phi_j, \quad (20)$$

and of the outer solution, \mathbf{q}^- , which can be a Dirichlet boundary condition that depends on the inner state, $\mathbf{q}^-(\mathbf{q}^+)$, or the discrete solution on a neighbor element,

$$\mathbf{q}^- = \sum_{j=1}^{\text{NDOF}^e} \mathbf{q}_j^N \phi_j^-, \quad (21)$$

where the quantities \mathbf{q}_j^N , ϕ_j^- and NDOF^e correspond to the coefficients of the solution, the values of the basis functions, and the number of degrees of freedom on a neighbor element, respectively. Several advective numerical fluxes are available in the finite volume literature [35].

When solving advection-diffusion PDEs, such as the Navier-Stokes equations, we also need a way to define the numerical trace of the solution, $\hat{\mathbf{q}}$, and the diffusive numerical flux, $\hat{\mathbf{f}}^\nu$. The former usually has a linear dependency on the solution on both sides of the interface [34], $\hat{\mathbf{q}}(\mathbf{q}^+, \mathbf{q}^-)$, and the latter can be classified as compact or non-compact depending on its dependencies.

The diffusive numerical flux is said to be compact if, besides depending on \mathbf{q}^+ , \mathbf{q}^- and \vec{n} , it also depends on the local gradients of the discrete solution on both sides of the surface $\partial\Omega^e$,

$$\hat{\mathbf{f}}^\nu = \hat{\mathbf{f}}^\nu(\mathbf{q}^+, \vec{\nabla} \mathbf{q}^+, \mathbf{q}^-, \vec{\nabla} \mathbf{q}^-, \vec{n}). \quad (22)$$

Several compact fluxes are available in the literature, such as the Interior Penalty (IP) flux [36] or the Bassi-Rebay 2 (BR2) flux [37]. On the other hand, the diffusive numerical flux is said to be non-compact if it depends on the DG discretized gradients on both sides of the surface $\partial\Omega^e$,

$$\hat{\mathbf{f}}^\nu = \hat{\mathbf{f}}^\nu(\mathbf{q}^+, \vec{\mathbf{g}}^+, \mathbf{q}^-, \vec{\mathbf{g}}^-, \vec{n}). \quad (23)$$

The Bassi-Rebay 1 (BR1) flux [38] is an example of a non-compact diffusive numerical flux.

In this paper, we restrict the analysis to compact diffusive numerical fluxes, as they link each element only with its neighbors. Non-compact diffusive numerical fluxes link each element with the neighbors of its neighbors. As a result, compact viscous numerical fluxes lead to sparser matrices that need less storage and whose matrix operations require fewer floating point operations.

In the DGSEM [13, 39], the tessellation is performed with non-overlapping quadrilateral ($d = 2$) or hexahedral ($d = 3$) elements, whose physical coordinates are obtained from a reference element in $[-1, 1]^d$ with a high-order mapping of order M ,

$$\vec{x}^e = \vec{x}^e(\vec{\xi}) \in \mathcal{P}^M, \quad \vec{\xi} = (\xi, \eta, \zeta) \in [-1, 1]^3. \quad (24)$$

The high-order mapping allows one to describe curved boundaries accurately, and to evaluate the integrals numerically by means of a Gaussian quadrature rule. In the DGSEM, we use a *non-overintegrated* quadrature of order N ,

$$\int_{\Omega^e} f d\Omega^e = \int_{-1}^1 \int_{-1}^1 \int_{-1}^1 J f d\xi d\eta d\zeta \approx \int_{\Omega^e} f d\Omega^e = \sum_{i,j,k=0}^N J_{ijk} w_i w_j w_k f(\vec{\xi}_{i,j,k}), \quad (25)$$

where w_i , w_j and w_k are the quadrature weights, $\vec{\xi}_{ijk}$ are the quadrature nodes, and J is the Jacobian of the transformation [13].

Furthermore, in the DGSEM the polynomial basis functions, ϕ_j , are tensor-product reconstructions of Lagrange interpolating polynomials on the quadrature points in each local coordinate direction:

$$\mathbf{q}^N(\vec{\xi}) = \sum_{n=1}^{\text{NDOF}^e} \mathbf{q}_n^N \phi_n(\vec{\xi}) = \sum_{i,j,k=0}^N \mathbf{q}_{i,j,k}^N \ell_i^\xi(\xi) \ell_j^\eta(\eta) \ell_k^\zeta(\zeta), \quad (26)$$

and the Lagrange polynomials are

$$\ell_i^\xi(\xi) = \prod_{\substack{m=0 \\ m \neq i}}^{N_1} \frac{\xi - \xi_m}{\xi_i - \xi_m}. \quad (27)$$

The standard choices for the quadrature rule are the Legendre-Gauss and the Legendre-Gauss-Lobatto nodes [13] (usually called only Gauss or Gauss-Lobatto points, respectively). Figure 1 shows the Lagrange interpolating polynomials on both quadrature rules for a $d = 1$ discretization with $N = 4$. Note that the Lagrange interpolating polynomials are discretely orthogonal,

$$\ell_i^\xi(\xi_j) = \delta_{ij}. \quad (28)$$

Therefore, all basis functions take a nonzero value on the boundary when using Gauss nodes, whereas only one basis function takes a value on each boundary when using Gauss-Lobatto nodes.

Replacing the integrals by quadrature rules and the basis functions by tensor-product Lagrange polynomials in (18) and (19), the DGSEM version of system (12) reads

$$\begin{cases} J_j w_j \partial_t \mathbf{q}_j^N - \int_{\Omega^e}^N \vec{\mathbf{f}}^N \cdot \vec{\nabla} \phi_j d\Omega^e + \int_{\partial\Omega^e}^N \hat{\mathbf{f}} \phi_j dS^e = \mathbf{0}, \\ - \int_{\Omega^e}^N \mathbf{q}^N \vec{\nabla} \phi_j d\Omega^e + \int_{\partial\Omega^e}^N \phi_j \hat{\mathbf{q}} \vec{n} dS^e = J_j w_j \vec{\mathbf{g}}_j^N. \end{cases} \quad (29a)$$

$$\quad (29b)$$

Equation (29) is valid for every degree of freedom of each element. It is possible to gather the contributions of all degrees of freedom and write the nonlinear system

$$\underline{\mathbf{M}} \frac{\partial \mathbf{Q}^N}{\partial t} + \mathbf{H}^N(\mathbf{Q}^N) = \mathbf{0}, \quad (30)$$

where $\underline{\mathbf{M}}$ is the so-called mass matrix, \mathbf{Q}^N is the vector that contains the solution on all the degrees of freedom of the discretization, and $\mathbf{H}^N(\cdot)$ is a nonlinear operator that contains all the DGSEM operations.

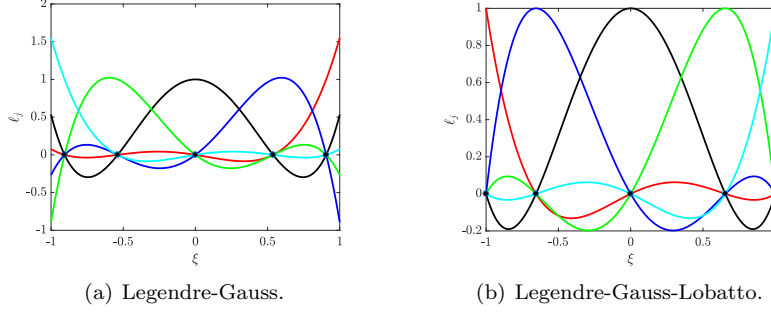


Figure 1: Lagrange interpolating polynomials on Legendre-Gauss and Legendre-Gauss-Lobatto points.

2.3. Time-Implicit DGSEM

We replace the time derivative in (30) by an implicit time integration scheme,

$$\frac{\partial \mathbf{Q}^N}{\partial t} \leftarrow \frac{\delta \mathbf{Q}^N}{\delta t}(\mathbf{Q}_{s+1}^N, \mathbf{Q}_s^N, \dots), \quad (31)$$

where the operator $\delta \mathbf{Q}^N / \delta t$ is a function of the solution on the next time step, \mathbf{Q}_{s+1}^N (the unknown), the current time step, \mathbf{Q}_s^N , and possibly previous time steps. Equation (30) can then be rewritten as

$$\underline{\mathbf{M}} \frac{\delta \mathbf{Q}^N}{\delta t}(\mathbf{Q}_{s+1}^N, \mathbf{Q}_s^N, \dots) + \mathbf{H}^N(\mathbf{Q}_{s+1}^N) = \mathbf{0}, \quad (32)$$

$$\mathbf{R}^N(\mathbf{Q}_{s+1}^N) = \mathbf{0}, \quad (33)$$

where the nonlinear operator \mathbf{H}^N is evaluated on the unknown solution, \mathbf{Q}_{s+1}^N .

The system of nonlinear equations, (33), can be solved with Newton's method. Using a Taylor expansion and neglecting terms with high-order derivatives the problem yields

$$\underline{\mathbf{A}} \Delta \mathbf{Q}^N = \mathbf{B}, \quad (34)$$

where $\underline{\mathbf{A}} = \partial \mathbf{R}^N / \partial \mathbf{Q}^N(\tilde{\mathbf{Q}}_{s+1}^N)$ is the Jacobian matrix, $\mathbf{B} = -\mathbf{R}(\tilde{\mathbf{Q}}_{s+1}^N)$ is the right-hand-side (RHS), and $\tilde{\mathbf{Q}}_{s+1}^N$ is an approximation to the unknown solution, \mathbf{Q}_{s+1}^N . Equation (34) is a linear system that must be solved multiple times to obtain better approximations of $\mathbf{Q}_{s+1}^N \leftarrow \tilde{\mathbf{Q}}_{s+1}^N + \Delta \mathbf{Q}^N$.

In following sections we derive the analytical expressions for the Jacobian matrix of a DGSEM discretization. To do that, we part from the DGSEM discretization (29) and linearize locally to obtain expressions that depend linearly on $\Delta \mathbf{q}^N$.

2.3.1. Advective Terms

To facilitate the derivation, let us first consider the purely advective equations with the temporal term (e.g. the compressible Euler equations of gas dynamics). The first step is to linearize the advective flux using a Taylor expansion,

$$\vec{\mathbf{f}}^a(\mathbf{q}) = \vec{\mathbf{f}}^a(\mathbf{q}_0) + \frac{\partial \vec{\mathbf{f}}^a}{\partial \mathbf{q}} \Delta \mathbf{q} + \mathcal{O}((\Delta \mathbf{q})^2) \quad (35)$$

$$\approx \vec{\mathbf{f}}^a(\mathbf{q}_0) + \underline{\mathbf{J}}^a \Delta \mathbf{q}, \quad (36)$$

where $\underline{\mathbf{J}}^a$ is the Jacobian of the advective flux evaluated with \mathbf{q}_0 .

A linearized expression for the advective numerical flux of an internal interface can be obtained in the same way, now taking into account that it depends on the solution on both sides of the interface,

$$\begin{aligned} \hat{\mathbf{f}}^a(\mathbf{q}^+, \mathbf{q}^-, \tilde{n}) \Big|_{\partial\Omega \setminus \Gamma} &= \hat{\mathbf{f}}^a(\mathbf{q}_0^+, \mathbf{q}_0^-, \tilde{n}) + \frac{\partial \hat{\mathbf{f}}^a}{\partial \mathbf{q}^+} \Delta \mathbf{q}^+ + \frac{\partial \hat{\mathbf{f}}^a}{\partial \mathbf{q}^-} \Delta \mathbf{q}^- + \mathcal{O}(\max((\Delta \mathbf{q}^+)^2, (\Delta \mathbf{q}^-)^2)) \\ &\approx \hat{\mathbf{f}}^a(\mathbf{q}_0^+, \mathbf{q}_0^-, \tilde{n}) + \hat{\mathbf{f}}_{\mathbf{q}^+}^a \Delta \mathbf{q}^+ + \hat{\mathbf{f}}_{\mathbf{q}^-}^a \Delta \mathbf{q}^-. \end{aligned} \quad (37)$$

In (37), $\hat{\mathbf{f}}_{\mathbf{q}^+}^a$ and $\hat{\mathbf{f}}_{\mathbf{q}^-}^a$ denote the Jacobians of the advective numerical flux function with respect to \mathbf{q}^+ and \mathbf{q}^- , respectively, evaluated in \mathbf{q}_0^+ and \mathbf{q}_0^- .

When the face of an element belongs to a physical domain boundary, $\partial\Omega \subseteq \Gamma$, the solution on the outer side of the face may depend on the solution on the inner side because of the boundary condition, $\mathbf{q}^-(\mathbf{q}^+)$. Therefore, the numerical flux function only depends on the solution on the inner side of the face, $\hat{\mathbf{f}}^a(\mathbf{q}^+, \tilde{n})$. As a consequence, (37) on a domain boundary is actually

$$\hat{\mathbf{f}}^a(\mathbf{q}^+, \tilde{n}) \Big|_{\partial\Omega \cap \Gamma} \approx \hat{\mathbf{f}}^a(\mathbf{q}_0^+, \tilde{n}) + (\hat{\mathbf{f}}_{\mathbf{q}^+}^a + \hat{\mathbf{f}}_{\mathbf{q}^-}^a \mathbf{q}_{\mathbf{q}^+}^-) \Delta \mathbf{q}^+, \quad (38)$$

where $\mathbf{q}_{\mathbf{q}^+}^- = \partial \mathbf{q}^- / \partial \mathbf{q}^+$ is the Jacobian of the Dirichlet boundary condition.

Inserting (36), (37) and (38) into (29a), we obtain

$$\begin{aligned} J_j w_j \partial_t \mathbf{q}_j^N + \left(- \int_{\Omega^e} (\underline{\mathbf{J}}^a \phi)_r \cdot \vec{\nabla} \phi_j d\Omega^e + \int_{\partial\Omega^e} \hat{\mathbf{f}}_{\mathbf{q}^+}^a \phi_r \phi_j dS + \int_{\partial\Omega^e \cap \Gamma} \hat{\mathbf{f}}_{\mathbf{q}^+}^a \mathbf{q}_{\mathbf{q}^+}^- \phi_r \phi_j dS \right) \Delta \mathbf{q}_r^N \\ + \left(\int_{\partial\Omega^e \setminus \Gamma} \hat{\mathbf{f}}_{\mathbf{q}^-}^a \phi_r^- \phi_j dS \right) \Delta \mathbf{q}_r^N = \hat{\mathbf{b}}_j^a, \end{aligned} \quad (39)$$

where we are using the Einstein notation convention with the index r to simplify the expression. Note that ϕ_r^- is the shape function that corresponds to the degree of freedom r of an external element ($\neq e$), \mathbf{q}_r^N is the solution state vector on that external degree of freedom r , and $\hat{\mathbf{b}}_j^a$ is the advective contribution to the right-hand-side that only depends on known values of the solution (\mathbf{q}_0^N).

The first term of (39) contributes to the diagonal blocks of the Jacobian matrix, and to the RHS in amounts that depend on the discretization of the time derivative. The second term of (39) contributes to the diagonal blocks of the Jacobian matrix as it multiplies the variation of the solution of the element. Finally, the third term of (39) contributes to the off-diagonal blocks of the matrix as it multiplies the solution on neighbor elements.

2.3.2. Diffusive Terms

We first consider (29a) without the time derivative and without the advective fluxes to facilitate the analysis. Rewriting (29a) with the explicit dependencies for a compact scheme yields

$$\int_{\Omega^e} \vec{\mathbf{f}}^\nu(\mathbf{q}^N, \vec{\mathbf{g}}^N) \cdot \vec{\nabla} \phi_j d\Omega^e - \int_{\partial\Omega^e} \hat{\mathbf{f}}^\nu(\mathbf{q}^+, \vec{\nabla} \mathbf{q}^+, \mathbf{q}^-, \vec{\nabla} \mathbf{q}^-, \tilde{n}) \phi_j d\Omega^e = \mathbf{0}, \quad (40)$$

As for the advective terms, we start by obtaining linearized versions of the viscous flux, which now depends on \mathbf{q} and $\vec{\mathbf{g}}$,

$$\begin{aligned} \vec{\mathbf{f}}^\nu(\mathbf{q}, \vec{\mathbf{g}}) &= \vec{\mathbf{f}}^\nu(\mathbf{q}_0, \vec{\mathbf{g}}_0) + \frac{\partial \vec{\mathbf{f}}^\nu}{\partial \mathbf{q}} \Delta \mathbf{q} + \frac{\partial \vec{\mathbf{f}}^\nu}{\partial \vec{\mathbf{g}}} \Delta \vec{\mathbf{g}} + \mathcal{O}(\max((\Delta \mathbf{q})^2, (\Delta \vec{\mathbf{g}})^2)) \\ &\approx \vec{\mathbf{f}}^\nu(\mathbf{q}_0, \vec{\mathbf{g}}_0) + \underline{\mathbf{J}}^\nu \Delta \mathbf{q} + \underline{\mathbf{G}}^\nu \Delta \vec{\mathbf{g}}, \end{aligned} \quad (41)$$

and of the viscous numerical flux,

$$\begin{aligned}
\hat{\mathbf{f}}^\nu(\mathbf{q}^+, \vec{\nabla}\mathbf{q}^+, \mathbf{q}^-, \vec{\nabla}\mathbf{q}^-, \vec{n}) &= \hat{\mathbf{f}}^\nu(\mathbf{q}_0^+, \vec{\nabla}\mathbf{q}_0^+, \mathbf{q}_0^-, \vec{\nabla}\mathbf{q}_0^-, \vec{n}) \\
&+ \frac{\partial \hat{\mathbf{f}}^\nu}{\partial \mathbf{q}^+} \Delta \mathbf{q}^+ + \frac{\partial \hat{\mathbf{f}}^\nu}{\partial \vec{\nabla}\mathbf{q}^+} \Delta(\vec{\nabla}\mathbf{q}^+) \\
&+ \frac{\partial \hat{\mathbf{f}}^\nu}{\partial \mathbf{q}^-} \Delta \mathbf{q}^- + \frac{\partial \hat{\mathbf{f}}^\nu}{\partial \vec{\nabla}\mathbf{q}^-} \Delta(\vec{\nabla}\mathbf{q}^-) + \mathcal{O}(\max((\Delta \mathbf{q}^+)^2, (\Delta \mathbf{q}^-)^2)) \\
&\approx \hat{\mathbf{f}}_0^\nu + \hat{\mathbf{f}}_{\mathbf{q}^+}^\nu \Delta \mathbf{q}^+ + \hat{\mathbf{f}}_{\vec{\nabla}\mathbf{q}^+}^\nu \Delta(\vec{\nabla}\mathbf{q}^+) + \hat{\mathbf{f}}_{\mathbf{q}^-}^\nu \Delta \mathbf{q}^- + \hat{\mathbf{f}}_{\vec{\nabla}\mathbf{q}^-}^\nu \Delta(\vec{\nabla}\mathbf{q}^-).
\end{aligned} \tag{42}$$

Inserting (41) and (42) into (40), and again replacing the functions by the corresponding polynomial expansions, yields

$$\begin{aligned}
&\left(\int_{\Omega^e}^N (\underline{\mathbf{J}}^\nu \phi)_r \cdot \vec{\nabla} \phi_j d\Omega^e \right) \Delta \mathbf{q}_r^N + \left(\int_{\Omega^e}^N (\underline{\mathbf{G}} \phi)_m \cdot \vec{\nabla} \phi_j d\Omega^e \right) \cdot \Delta \underline{\mathbf{g}}_m^N \\
&- \left(\int_{\partial\Omega^e \setminus \Gamma}^N (\hat{\mathbf{f}}_{\mathbf{q}^+}^\nu \phi_r + \hat{\mathbf{f}}_{\vec{\nabla}\mathbf{q}^+}^\nu \cdot \vec{\nabla} \phi_r) \phi_j d\Omega^e + \int_{\partial\Omega^e \cap \Gamma}^N \left(\frac{\partial \hat{\mathbf{f}}_\Gamma^\nu}{\partial \mathbf{q}^+} \phi_r + \frac{\partial \hat{\mathbf{f}}_\Gamma^\nu}{\partial \vec{\nabla}\mathbf{q}^+} \cdot \vec{\nabla} \phi_r \right) \phi_j d\Omega^e \right) \Delta \mathbf{q}_r^N \\
&- \left(\int_{\partial\Omega^e \setminus \Gamma}^N (\hat{\mathbf{f}}_{\mathbf{q}^-}^\nu \phi_r^- + \hat{\mathbf{f}}_{\vec{\nabla}\mathbf{q}^-}^\nu \cdot \vec{\nabla} \phi_r^-) \phi_j d\Omega^e \right) \Delta \mathbf{q}_r^N = \hat{\mathbf{b}}_j^\nu, \tag{43}
\end{aligned}$$

where Einstein notation is again used for the indexes r and m . The Jacobian of the numerical fluxes on the faces that belong to the physical boundaries, $\partial\Omega^e \cap \Gamma$, can be expressed as

$$\frac{\partial \hat{\mathbf{f}}_\Gamma^\nu}{\partial \mathbf{q}^+} = \hat{\mathbf{f}}_{\mathbf{q}^+}^\nu + \hat{\mathbf{f}}_{\mathbf{q}^-}^\nu \mathbf{q}_{\mathbf{q}^+}^- + \hat{\mathbf{f}}_{\vec{\nabla}\mathbf{q}^-}^\nu (\vec{\nabla}\mathbf{q}^-)_{\mathbf{q}^+}, \text{ and} \tag{44}$$

$$\frac{\partial \hat{\mathbf{f}}_\Gamma^\nu}{\partial \vec{\nabla}\mathbf{q}^+} = \hat{\mathbf{f}}_{\vec{\nabla}\mathbf{q}^+}^\nu + \hat{\mathbf{f}}_{\vec{\nabla}\mathbf{q}^-}^\nu (\vec{\nabla}\mathbf{q}^-)_{\vec{\nabla}\mathbf{q}^+}, \tag{45}$$

where $\mathbf{q}_{\mathbf{q}^+}^-$ is again the Jacobian of the Dirichlet boundary condition, and $(\vec{\nabla}\mathbf{q}^-)_{\mathbf{q}^+}$ and $(\vec{\nabla}\mathbf{q}^-)_{\vec{\nabla}\mathbf{q}^+}$ are the Jacobians of the Neumann boundary condition.

Since we want an expression with linear dependencies on $\Delta \mathbf{q}^N$ to construct $\underline{\mathbf{A}}$, we now have to rewrite $\underline{\mathbf{g}}_m^N$ in (43) with its dependencies on \mathbf{q}^N . This can be done by performing the same local linearization procedure on (29b). Since in all classical viscous numerical fluxes [34] $\hat{\mathbf{q}}$ is linear with respect to the solution on both sides of the interface, \mathbf{q}^+ and \mathbf{q}^- , (29b) can be reduced to

$$\begin{aligned}
J_m w_m \underline{\mathbf{g}}_m^N &= \left(- \int_{\Omega}^N \phi_r \vec{\nabla} \phi_m d\Omega + \int_{\partial\Omega}^N \hat{\mathbf{q}}_{\mathbf{q}^+} \phi_r \phi_m \vec{n} dS + \int_{\partial\Omega \cap \Gamma}^N \hat{\mathbf{q}}_{\mathbf{q}^-} \mathbf{q}_{\mathbf{q}^+}^- \phi_r \phi_m \vec{n} dS \right) \mathbf{q}_r^N \\
&+ \left(\int_{\partial\Omega \setminus \Gamma}^N \hat{\mathbf{q}}_{\mathbf{q}^-} \phi_r^- \phi_m \vec{n} dS \right) \mathbf{q}_r^N. \tag{46}
\end{aligned}$$

2.4. Static Condensation

The static-condensation method, or Guyan reduction [24], is a well-known technique to reduce the size of linear systems that can be written in blocks as

$$\begin{bmatrix} \underline{\mathbf{B}} & \underline{\mathbf{C}} \\ \underline{\mathbf{D}} & \underline{\mathbf{E}} \end{bmatrix} \begin{bmatrix} \mathbf{X}_1 \\ \mathbf{X}_2 \end{bmatrix} = \begin{bmatrix} \mathbf{F}_1 \\ \mathbf{F}_2 \end{bmatrix}, \tag{47}$$

where $\underline{\mathbf{B}} \in \mathbb{R}^{n_1 \times n_1}$, $\underline{\mathbf{C}} \in \mathbb{R}^{n_1 \times n_2}$, $\underline{\mathbf{D}} \in \mathbb{R}^{n_2 \times n_1}$, and $\underline{\mathbf{E}} \in \mathbb{R}^{n_2 \times n_2}$.

We start by performing block Gauss elimination, which can be summarized as multiplying the system (47) on the left by the matrix

$$\begin{bmatrix} \underline{\mathbf{I}} & -\underline{\mathbf{C}}\underline{\mathbf{E}}^{-1} \\ \mathbf{0} & \underline{\mathbf{I}} \end{bmatrix}, \tag{48}$$

to obtain

$$\begin{bmatrix} \underline{\mathbf{B}} - \underline{\mathbf{C}}\underline{\mathbf{E}}^{-1}\underline{\mathbf{D}} & \mathbf{0} \\ \underline{\mathbf{D}} & \underline{\mathbf{E}} \end{bmatrix} \begin{bmatrix} \mathbf{X}_1 \\ \mathbf{X}_2 \end{bmatrix} = \begin{bmatrix} \mathbf{F}_1 - \underline{\mathbf{C}}\underline{\mathbf{E}}^{-1}\mathbf{F}_2 \\ \mathbf{F}_2 \end{bmatrix}. \quad (49)$$

In (49), the system of equations for \mathbf{X}_1 is decoupled from the rest of the system with a block of zeros in the upper off-diagonal. As a result, the original system can be solved in two steps:

1. Solve the statically-condensed system for \mathbf{X}_1 ,

$$[\underline{\mathbf{B}} - \underline{\mathbf{C}}\underline{\mathbf{E}}^{-1}\underline{\mathbf{D}}]\mathbf{X}_1 = \mathbf{F}_1 - \underline{\mathbf{C}}\underline{\mathbf{E}}^{-1}\mathbf{F}_2, \quad (50)$$

where the condensed matrix is also known as the Schur complement of the original global matrix.

2. Compute \mathbf{X}_2 as a function of \mathbf{X}_1 ,

$$\mathbf{X}_2 = \underline{\mathbf{E}}^{-1}(\mathbf{F}_2 - \underline{\mathbf{D}}\mathbf{X}_1). \quad (51)$$

This approach is computationally efficient if n_1 is small and the matrix $\underline{\mathbf{E}}$ is easily invertible. In fact, the action of $\underline{\mathbf{E}}^{-1}$ on a vector is needed in (50) to construct the statically condensed system matrix (n_1 times, i.e. the number of columns of $\underline{\mathbf{D}}$) and to construct the statically-condensed RHS (one time), and in (51) to recover \mathbf{X}_2 (one time).

The static-condensation method has been applied to time-implicit Continuous Galerkin (CG) [25–27] and Discontinuous Galerkin (DG) [28–30] methods, where the linear system is of the form

$$\underline{\mathbf{A}}\mathbf{Q} = \mathbf{B} \quad (52)$$

(note that the delta symbol is omitted for readability, $\Delta\mathbf{Q} \leftarrow \mathbf{Q}$, which does not necessarily imply that we are dealing with linear fluxes).

In what follows, we present a brief description of the state-of-the-art implementations of the static-condensation method for CG and DG, and then we show how static condensation can be applied to the GL-DGSEM in an efficient manner.

2.4.1. Continuous Galerkin Methods

Static condensation was first used by Fraeijs in 1965 [25] to reduce the size of the linear system that results from time-implicit Finite Element discretizations. In general, in medium-to-high order ($N \geq 2$) continuous Galerkin (CG) discretizations, it is easy to reorganize the linear system (52) as

$$\begin{bmatrix} \underline{\mathbf{A}}_{bb} & \underline{\mathbf{A}}_{ib} \\ \underline{\mathbf{A}}_{bi} & \underline{\mathbf{A}}_{ii} \end{bmatrix} \begin{bmatrix} \mathbf{Q}_b \\ \mathbf{Q}_i \end{bmatrix} = \begin{bmatrix} \mathbf{B}_b \\ \mathbf{B}_i \end{bmatrix}, \quad (53)$$

where \mathbf{Q}_b is the solution on the degrees of freedom that sit on the element boundaries (interfaces), and \mathbf{Q}_i is the solution on the inner degrees of freedom. Moreover, $\underline{\mathbf{A}}_{bb}$ is the boundary-to-boundary matrix, $\underline{\mathbf{A}}_{ib}$ is the interior-to-boundary matrix, $\underline{\mathbf{A}}_{bi}$ is the boundary-to-interior matrix, and $\underline{\mathbf{A}}_{ii}$ is the interior-to-interior matrix.

Note that system (53) is equivalent to system (47), for

$$\begin{bmatrix} \underline{\mathbf{B}} & \underline{\mathbf{C}} \\ \underline{\mathbf{D}} & \underline{\mathbf{E}} \end{bmatrix} \leftrightarrow \begin{bmatrix} \underline{\mathbf{A}}_{bb} & \underline{\mathbf{A}}_{ib} \\ \underline{\mathbf{A}}_{bi} & \underline{\mathbf{A}}_{ii} \end{bmatrix}, \quad \begin{bmatrix} \mathbf{X}_1 \\ \mathbf{X}_2 \end{bmatrix} \leftrightarrow \begin{bmatrix} \mathbf{Q}_b \\ \mathbf{Q}_i \end{bmatrix}, \quad \begin{bmatrix} \mathbf{F}_1 \\ \mathbf{F}_2 \end{bmatrix} \leftrightarrow \begin{bmatrix} \mathbf{B}_b \\ \mathbf{B}_i \end{bmatrix}, \quad (54)$$

and it can be solved using the same two-step procedure. Furthermore, since the coupling between elements in CG occurs only through the (shared) degrees of freedom on element interfaces, the matrix $\underline{\mathbf{A}}_{ii}$ has a block diagonal structure, which makes it easy to invert in a local manner.

Static condensation has also been used by Karniadakis and Sherwin [26] and Vos et al. [27] for high-order CG methods, who have shown that the computational efficiency is increased when the order of the approximation (N) is increased because the relative size of the condensed system, $n_1/(n_1 + n_2)$, decreases with N .

2.4.2. Discontinuous Galerkin Methods

We now detail how static condensation has been used with high-order DG methods. Unlike CG methods, DG methods may couple all the degrees of freedom of an element with the degrees of freedom of its neighbors (see (39) and (43)), or neighbors of neighbors (if a non-compact DG method is used), through the numerical flux functions. As a result, the static-condensation method is in general not directly applicable.

The first implementation of a static-condensation DG scheme was presented by Sherwin et al. [28], who were able to make a modal DG scheme suitable for static condensation by using C^0 -type expansions for the basis functions on element boundaries and bubble functions for the inner modes. This choice of basis resembles the one used in p -FEM, a type of continuous Galerkin methods. Consequently, the linear system that is produced from the implicit time-integration of the modified DG scheme can also be arranged as the system (53), where the matrix $\underline{\mathbf{A}}_{ii}$ is also block diagonal. This proved to be advantageous since the statically condensed system was shown to be not only smaller in size but also cheap-to-compute and better conditioned than the global system.

Sherwin et al. [28] allege that an additional advantage of their statistically condensable DG is that the boundary conditions can be imposed through global lifting, as is in continuous Galerkin methods, hence reducing the number of degrees of freedom of the problem. This is useful to treat elliptic problems but it may need stabilization for hyperbolic equations.

The only drawback of Sherwin's approach is that the new specially tailored basis functions are neither orthogonal expansions nor tensor-product bases. Therefore, several advantages of such basis functions cannot be kept, such as the existence of diagonal mass matrices, sparser Jacobians, the possibility to evaluate the anisotropic truncation error estimator of [40], the ability to perform anisotropic p -adaptation [41], among others.

Another approach to perform static condensation in DG methods was developed simultaneously and independently from Sherwin's approach by Carrero and Cockburn et al. [29, 30] and is known as the Hybridizable Discontinuous Galerkin (HDG) method. This method imposes no restrictions on the choice of basis functions and has gained increased popularity in recent years [42, 43].

The HDG method expands the original DG system with a new unknown variable that only lives on the mesh skeleton, $\boldsymbol{\lambda}$ (typically the numerical trace of the solution, $\boldsymbol{\lambda} = \hat{\mathbf{q}}$), with which it is possible to statically condense it. The expanded system is

$$\begin{bmatrix} \underline{\mathbf{B}} & \underline{\mathbf{C}} \\ \underline{\mathbf{D}} & \underline{\mathbf{A}}_B \end{bmatrix} \begin{bmatrix} \boldsymbol{\Lambda} \\ \mathbf{Q} \end{bmatrix} = \begin{bmatrix} \mathbf{F}_1 \\ \mathbf{B} \end{bmatrix}, \quad (55)$$

where $\underline{\mathbf{A}}_B$ is a matrix formed by the diagonal blocks of matrix $\underline{\mathbf{A}}$, $\boldsymbol{\Lambda}$ is the sampled version of $\boldsymbol{\lambda}$, and $\underline{\mathbf{B}}$, $\underline{\mathbf{C}}$, $\underline{\mathbf{D}}$ and \mathbf{F}_1 are additional terms that contain the scattered information of the off-diagonal blocks of $\underline{\mathbf{A}}$. A similar approach is done by Petersen [44] for a space-time DG, where $\boldsymbol{\Lambda}$ are Lagrange multipliers.

Note that we kept almost the same notation of (52) in (55), but some variables were changed by the names they usually have in the HDG community. Therefore we have

$$\begin{bmatrix} \underline{\mathbf{B}} & \underline{\mathbf{C}} \\ \underline{\mathbf{D}} & \underline{\mathbf{E}} \end{bmatrix} \leftrightarrow \begin{bmatrix} \underline{\mathbf{B}} & \underline{\mathbf{C}} \\ \underline{\mathbf{D}} & \underline{\mathbf{A}}_B \end{bmatrix}, \quad \begin{bmatrix} \mathbf{X}_1 \\ \mathbf{X}_2 \end{bmatrix} \leftrightarrow \begin{bmatrix} \boldsymbol{\Lambda} \\ \mathbf{Q} \end{bmatrix}, \quad \begin{bmatrix} \mathbf{F}_1 \\ \mathbf{F}_2 \end{bmatrix} \leftrightarrow \begin{bmatrix} \mathbf{F}_1 \\ \mathbf{B} \end{bmatrix}. \quad (56)$$

The first formulations of the HDG method [29, 30] dealt with linear elliptic problems and imposed particular conditions, such as the requirement on the viscous numerical fluxes to be adjoint-consistent (see for example [34]). When solving nonlinear conservation laws, additional constraints are imposed for a DG method to be hybridizable with $\boldsymbol{\lambda} = \hat{\mathbf{q}}$. For example, the numerical flux is restricted to the form [31, 32]

$$\hat{\mathbf{f}} = \tilde{\mathbf{f}}(\hat{\mathbf{q}}) \cdot \vec{n} + \underline{\mathbf{S}}(\mathbf{q}^N, \hat{\mathbf{q}})(\mathbf{q}^N - \hat{\mathbf{q}}), \quad (57)$$

where \mathbf{q}^N is the solution on the element e , $\hat{\mathbf{q}}$ is the numerical trace of it, and $\underline{\mathbf{S}}$ is a stabilizing function. Some broadly used numerical flux functions, such as the Lax-Friedrichs flux, can be expressed in this form, but others (e.g. Roe) cannot.

Without the constraint (57), it would not be possible to condense the system as a function of $\hat{\mathbf{Q}}$. However, we would like to point out that, in purely advective nonlinear conservation laws, it is possible to use $\boldsymbol{\lambda} = \hat{\mathbf{f}}^a$ and ignore the restriction (57).

3. Statically Condensed GL-DGSEM

We now show that the GL-DGSEM is suitable for static condensation. In Section 3.1, we analyze and compare the Jacobian matrix sparsity patterns of time-implicit G-DGSEM and GL-DGSEM. From this analysis, it follows that the linear systems for the DGSEM on Gauss-Lobatto points can be directly organized as (53), where $\underline{\mathbf{A}}_{ii}$ is a block-diagonal matrix. Hence, static condensation can be directly and efficiently applied to the GL-DGSEM. In Section 3.2, we analyze the properties of the statically condensed GL-DGSEM system and detail its implementation.

3.1. Jacobian Sparsity Patterns

Following the methodology of Section 2.3, we first present the analysis for the advective terms and then for the viscous terms. Furthermore, the sparsity patterns of a seven-element 1D discretization of order $N = 9$ (Figure 2(a)) and an eight-element 3D discretization of order $N = 3$ (Figure 2(b)) will be illustrated in this section to simplify the analysis.

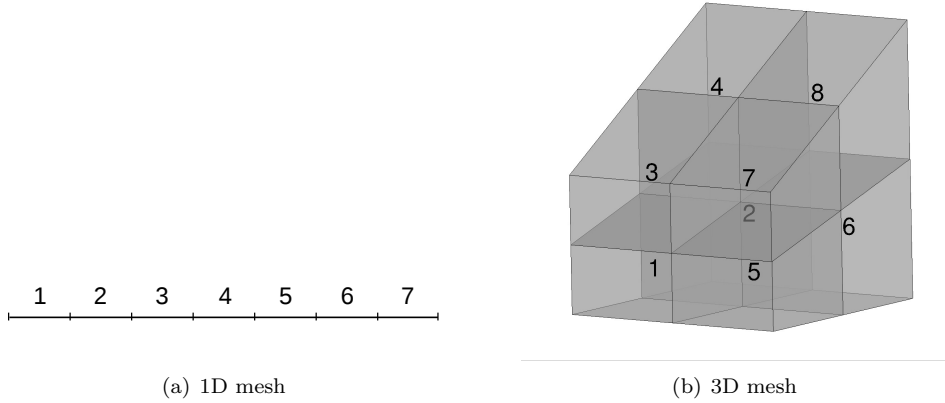


Figure 2: Meshes analyzed for sparsity patterns showing the element numbering.

3.1.1. Advective Terms

The entries of the Jacobian matrix are presented in (39) for a standard time-implicit DGSEM discretization of an advective conservation law. From (39), it can be inferred that the advective off-diagonal term (ODT_{jr}^a) that corresponds to the degree of freedom j of the element e , and the degree of freedom r of a certain neighbor element (i.e. the term that multiplies $\Delta \mathbf{q}_r^N$), is

$$\text{ODT}_{jr}^a = \int_{\partial\Omega^e \setminus \Gamma} \hat{\mathbf{f}}_{\mathbf{q}}^a \phi_r^- \phi_j \mathrm{d}S^e \quad (58)$$

This term is guaranteed to be zero if the basis functions, ϕ_j or ϕ_r^- , are zero on the element interface.

As explained in Section 2.2, if one uses Gauss nodes, all basis functions take nonzero values on the element interfaces. Therefore, ϕ_j and ϕ_r^+ always contribute to the surface integral (for any j and r). On the other hand, if one uses Gauss-Lobatto nodes, only the basis functions that correspond to interface degrees of freedom take nonzero values on the element interfaces. Therefore, ϕ_j and ϕ_r^+ only contribute to ODT_{jr}^a if

j and r are degrees of freedom that sit on the element boundary. See Figure 1 for details on how the basis functions look on the two node distributions.

The difference between the basis functions on Gauss and Gauss-Lobatto nodes causes different matrix sparsity patterns for the two node distributions, which are illustrated in Figure 3 for the 1D mesh of Figure 2(a) and a scalar ($n_{\text{cons}} = 1$) advection equation. Note that in the 1D DGSEM with Gauss nodes, all the degrees of freedom of a given element are coupled with the degrees of freedom of a neighbor element through entries in the corresponding off-diagonal block. Contrarily, in the DGSEM with Gauss-Lobatto nodes, only the boundary degrees of freedom are coupled through entries on the off-diagonal block. As a result, the 1D GL-DGSEM matrix is almost block-diagonal (there is only one entry in each off-diagonal block). Consequently, it is possible to reorganize the rows and columns that correspond to boundary degrees of freedom to obtain an equivalent linear system with the structure of (53), where A_{ii} is a block-diagonal matrix.

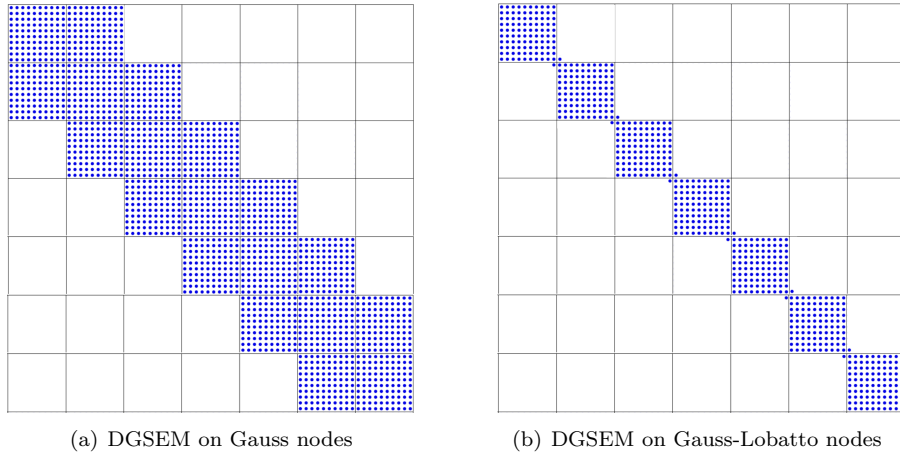


Figure 3: Sparsity patterns of system matrices for 1D scalar advective equations.

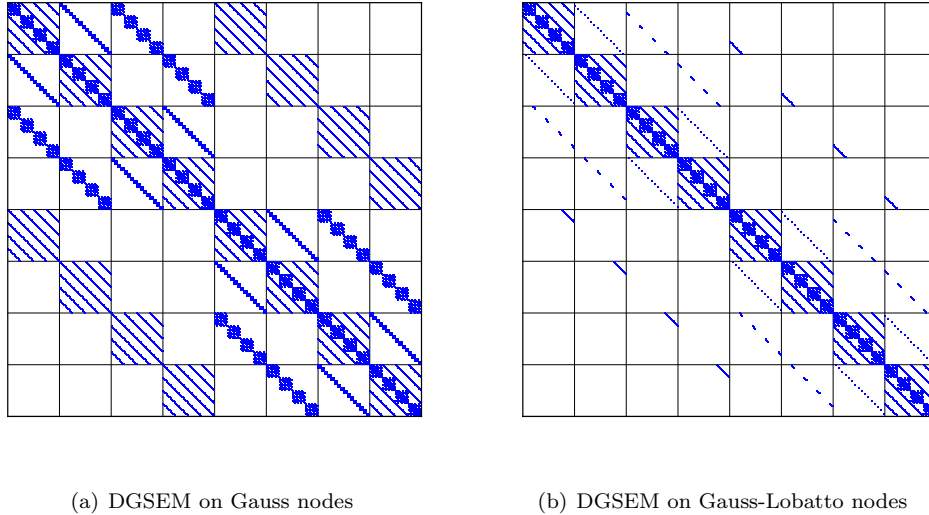


Figure 4: Sparsity patterns of system matrices for advective 3D single-equation discretizations.

Figure 4 shows that a similar behavior is observed for the 3D mesh of Figure 2(b). In this context, the sparsity patterns are also shown for a scalar PDE, where each pixel is an entry of the Jacobian matrix. In multi-equation PDEs, the sparsity pattern is very similar, but each pixel would contain an $n_{\text{cons}} \times n_{\text{cons}}$ matrix that is not necessarily dense. In 3D, the diagonal and off-diagonal blocks are no longer dense because of the tensor-product basis expansions. This can be exploited to reduce the storage requirements, especially for very high orders ($N > 3$).

In the 3D DGSEM with Gauss nodes all the degrees of freedom of a given element are coupled (through the off-diagonal block) with some degrees of freedom of the neighbor elements in a way that makes it impossible to reorganize the system as (53) with A_{ii} as a block-diagonal matrix. However, when Gauss-Lobatto nodes are used and the matrix is reorganized, A_{ii} is indeed a block-diagonal matrix since only the boundary degrees of freedom are coupled with other boundary degrees of freedom.

3.1.2. Diffusive Terms

The Jacobian entries produced by the diffusive terms of the PDE are computed from (43) and (46). Taking into account that the index m in (43) is used in an Einstein summation convention, the diffusive off-diagonal term (ODT_{jr}^ν) that corresponds to the degree of freedom j of the element e , and the degree of freedom r of a certain neighbor element (i.e. the term that multiplies $\Delta \mathbf{q}_r^N$), is

$$\text{ODT}_{jr}^\nu = \sum_{m=1}^{\text{NDOF}^e} \left[\frac{1}{J_m w_m} \left(\int_{\Omega^e} \mathbf{G}_m \phi_m \cdot \vec{\nabla} \phi_j d\Omega^e \right) \cdot \left(\int_{\partial\Omega^e \setminus \Gamma} \phi_r^- \phi_m \vec{n} dS^e \right) \right] - \int_{\partial\Omega^e \setminus \Gamma} \left(\hat{\mathbf{f}}_{\mathbf{q}^-}^\nu \phi_r^- + \hat{\mathbf{f}}_{\vec{\nabla} \mathbf{q}^-}^\nu \vec{\nabla} \phi_r^- \right) \phi_j d\Omega^e. \quad (59)$$

It is evident that (59) generates much denser off-diagonal blocks than the ones obtained for the advective terms. As a matter of fact, at first sight one could think that static condensation is not applicable to the time-implicit GL-DGSEM when diffusive terms are present. However, it is, as can be observed in Figure 5, which shows the resulting sparsity patterns for the 1D mesh of Figure 2(a).

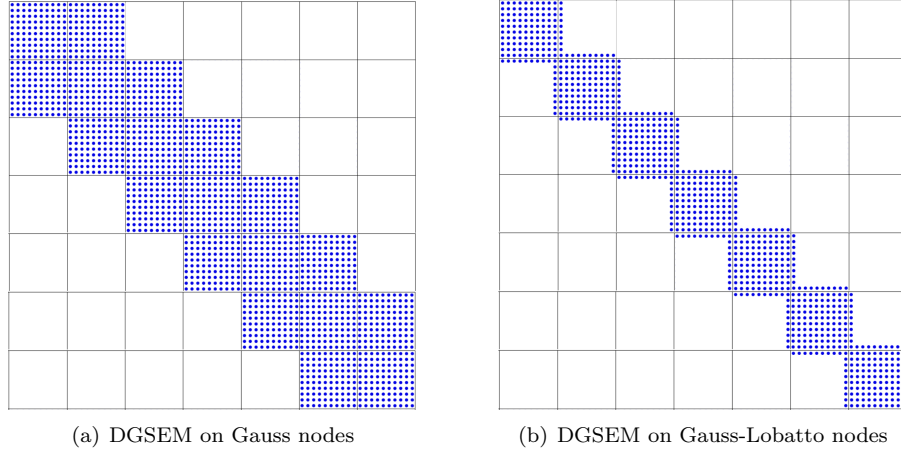


Figure 5: Sparsity patterns of system matrices for advection-diffusion 1D single-equation discretizations.

The 1D sparsity pattern for the DGSEM on Gauss nodes is the same as in the advective case, but there are substantial differences when Gauss-Lobatto nodes are used. To begin with, the first term of (59) takes nonzero values for any degree of freedom j of the element that is being analyzed, if and only if r corresponds to a boundary degree of freedom of a neighbor element, i.e. when $\phi_r^- \neq 0$. Moreover, the second term takes nonzero values for any r , if and only if $\phi_j \neq 0$, i.e. for a boundary degree of freedom of the analyzed element.

As a result, a whole row and a whole column of each off-diagonal block of the 1D system matrix is filled with nonzero values. These blocks are indeed denser than in the advective case, but the static-condensation method can still be applied with the same row/column reordering.

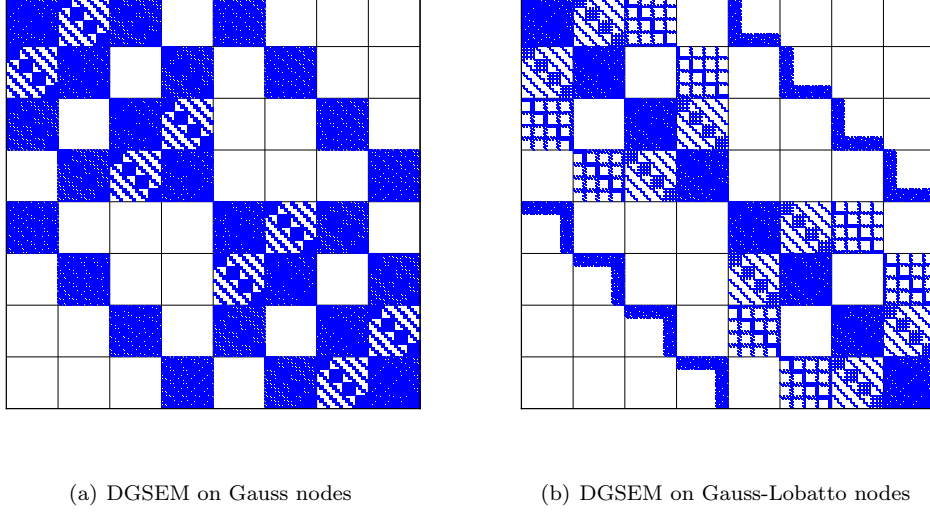


Figure 6: Sparsity patterns of system matrices for advection-diffusion 1D single-equation discretizations.

The 3D discretization is more complex than the 1D, but it retains similar properties. Figure 6 shows the sparsity pattern that is produced by the time-implicit DGSEM discretization of a scalar nonlinear advection-diffusion equation in the 3D mesh of Figure 2(b). As can be seen, both the diagonal and off-diagonal blocks are sparse because of the tensor-product basis expansions, but they are much denser than in the purely advective case. This is a consequence of the additional spatial derivatives. Moreover, it is again impossible to reorder the G-DGSEM matrix of Figure 6(a) to obtain a block-diagonal $\underline{\mathbf{A}}_{ii}$ matrix. In contrast, the matrix resulting from the Gauss-Lobatto discretization (Figure 6(b)) is suitable for static condensation. This is clearly seen from the appearance of some off-diagonal blocks, like the ones connecting elements 1-3 or 1-5. However, the off-diagonal blocks that connect elements 1-2 or 3-4 seem to have a more complicated sparsity pattern that does not allow to obtain block-diagonal matrices when reordering. This is just an artifact of the plotting. In fact, a detailed view of the part of the Jacobian that corresponds to elements 1 and 2 (Figure 7) reveals that only some of the degrees of freedom are coupled in the Gauss-Lobatto DGSEM.

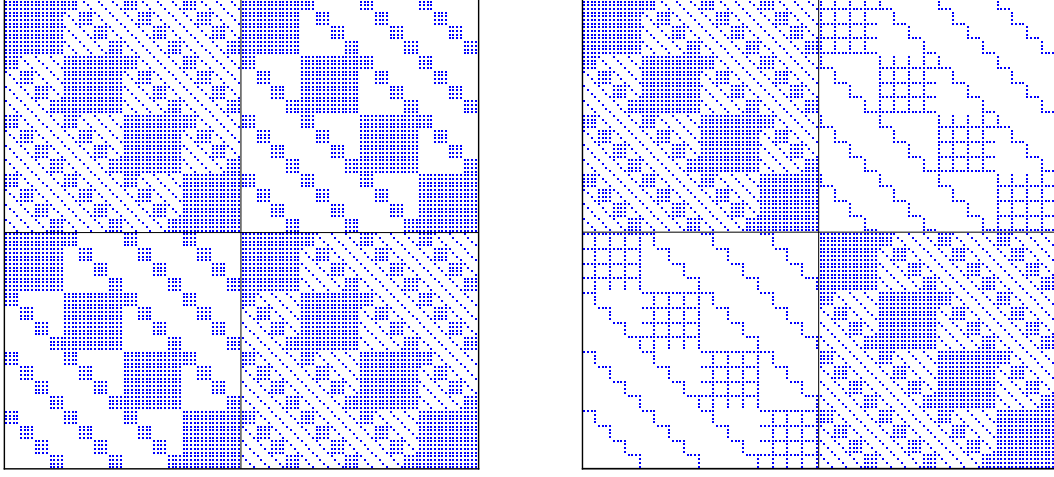
In summary, the off-diagonal blocks of a GL-DGSEM discretization only take nonzero values if

- j **and** r correspond to boundary degrees of freedom (advective case), or
- j **or** r correspond to boundary degrees of freedom (diffusive case).

In either case, the system can be reorganized as a Schur complement problem with $\underline{\mathbf{A}}_{ii}$ being a block-diagonal matrix.

3.2. Analysis and Implementation

As was shown in previous section, the linear system resulting from the GL-DGSEM discretization of an advection, diffusion or advection-diffusion conservation law can be reorganized and condensed to obtain a



(a) DGSEM on Gauss nodes

(b) DGSEM on Gauss-Lobatto nodes

Figure 7: Detail of the Jacobian blocks corresponding to elements 1 and 2.

new system of the form,

$$\begin{bmatrix} \underline{\mathbf{A}}_{bb} - \underline{\mathbf{A}}_{ib} \underline{\mathbf{A}}_{ii}^{-1} \underline{\mathbf{A}}_{bi} & \mathbf{0} \\ \underline{\mathbf{A}}_{bi} & \underline{\mathbf{A}}_{ii} \end{bmatrix} \begin{bmatrix} \mathbf{Q}_b \\ \mathbf{Q}_i \end{bmatrix} = \begin{bmatrix} \mathbf{B}_b - \underline{\mathbf{A}}_{ib} \underline{\mathbf{A}}_{ii}^{-1} \mathbf{B}_i \\ \mathbf{B}_i \end{bmatrix}, \quad (60)$$

where $\underline{\mathbf{A}}_{ii}$ is a block-diagonal matrix. In addition, as was shown in Section 2.4, this new linear system can be solved in two steps: the linear solve of the condensed system and the reconstruction of the solution on the inner degrees of freedom.

The construction of the condensed system is graphically represented in Figure 8 for the simple 3D mesh of Figure 2(b) and for the compressible Navier-Stokes equations ($n_{\text{cons}} = 5$).

A few remarks can be made.

- The blocks of matrix $\underline{\mathbf{A}}_{ii}$ keep the tensor-product sparsity and the whole matrix can be inverted locally (element by element).
- The condensed matrix keeps the diagonal dominance with a seemingly denser structure.
- In fact, the condensed system matrix exhibits element connectivities that were not spotted in the global matrices of last section: In spite of the use of a compact viscous numerical flux, there are off-diagonal entries that suggest a *neighbors of neighbors* coupling. This behavior is not observed in the purely advective case (not shown here).

The ratio of the condensed system size (n_1) to the global system size ($n_1 + n_2$) is a function of the polynomial order. Supposing p -isotropic discretizations, the maximum ratio is

$$\left. \frac{n_1}{n_1 + n_2} \right|_{\max} = \frac{(N+1)^d - (N-1)^d}{(N+1)^d}, \quad (61)$$

where d is the number of dimensions of the problem. Note that an advantage in the system size is only observed for $N > 1$.

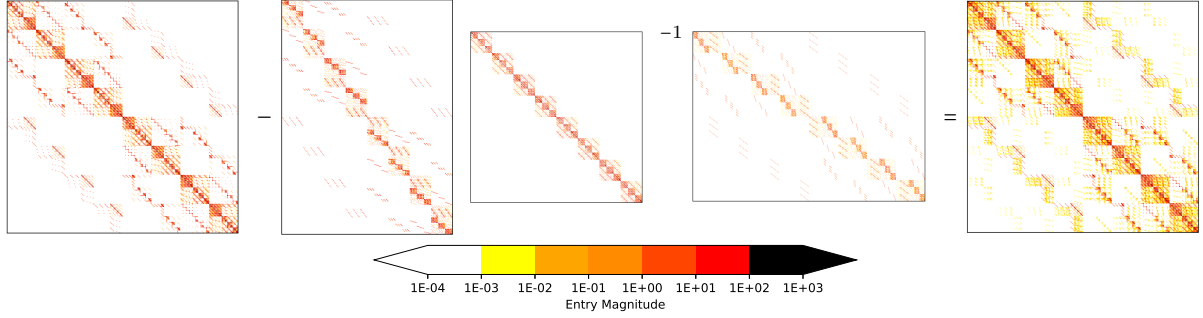


Figure 8: Matrix condensation operations for the 3D Navier-Stokes ($n_{\text{cons}} = 5$) case: $\underline{\mathbf{A}}_{bb} - \underline{\mathbf{A}}_{ib}\underline{\mathbf{A}}_{ii}^{-1}\underline{\mathbf{A}}_{bi} = \underline{\mathbf{A}}_C$. Every pixel corresponds to a matrix entry.

Table 1: Ratio of condensed system size to global system size

$d =$	1	2	3
$\frac{n_1}{n_1 + n_2}$	$\frac{2}{N+1}$	$\frac{4N}{(N+1)^2}$	$\frac{6N^2+2}{(N+1)^3}$

Figure 9 shows the ratio of the condensed system size to the global system size as a function of the polynomial order for p -isotropic discretizations in every element. The maximum ratio corresponds to the theoretical value that can be computed supposing that all the degrees of freedom on element boundaries contribute to off-diagonal blocks. The achievable ratio is problem-dependent (here for the diffuser mesh of Figure 2(b)). It is a function of how many element boundaries correspond to domain boundaries. Namely, the degrees of freedom on the domain boundaries only contribute to the diagonal blocks and, therefore, it is not necessary to include them in the \mathbf{Q}_b vector. As expected, the static-condensation method provides increasing advantages as the polynomial order is incremented.

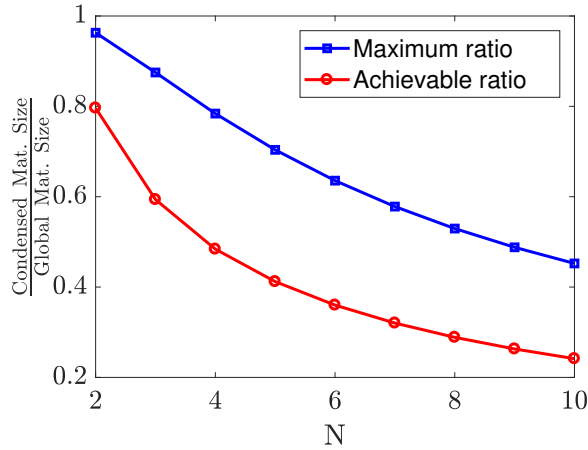


Figure 9: Ratio of condensed system size to global system size (3D diffuser example).

In the following section, a numerical example is presented that was obtained using an implementation of the static-condensation method for the GL-DGSEM. The Jacobian is computed analytically following the derivations of Section 2.3 and stored in four matrices that correspond to $\underline{\mathbf{A}}_{ii}$, $\underline{\mathbf{A}}_{bi}$, $\underline{\mathbf{A}}_{ib}$ and $\underline{\mathbf{A}}_{bb}$. To do

that, the mesh connectivities are preprocessed to obtain appropriate permutation indexes for each degree of freedom. The matrices $\underline{\mathbf{A}}_{bi}$, $\underline{\mathbf{A}}_{ib}$ and $\underline{\mathbf{A}}_{bb}$ are stored in sparse CSR formats and the blocks of $\underline{\mathbf{A}}_{ii}$ are stored as dense matrices. The matrix-matrix multiplications are performed with the routines provided by the BLAS libraries [45] and the individual blocks of $\underline{\mathbf{A}}_{ii}$ are inverted using the LU decomposition routines of the LAPACK [46] library with no regard of the tensor-product properties.

4. Numerical Example

In this section, we test the computational performance of the statically condensed time-implicit GL-DGSEM and compare it with the traditional (not statically condensed) time-implicit GL-DGSEM and a time-explicit GL-DGSEM. The flow past a cylinder at $\text{Re}_\infty = 30$ and $\text{Ma}_\infty = 0.2$ is simulated using polynomial orders that range between $N = 3$ and $N = 7$. The Lax-Friedrichs flux is used as the advective numerical flux, $\hat{\mathbf{f}}^a$, and the symmetric interior penalty method is used as the diffusive numerical flux, $\hat{\mathbf{f}}^v$ and $\hat{\mathbf{q}}$. All simulations were run in a 24-core Xeon broadwell e5-2690v4 and the Jacobians of the time-implicit simulations were computed analytically. Figure 10 shows the horizontal velocity contours and the mesh used for this test case.

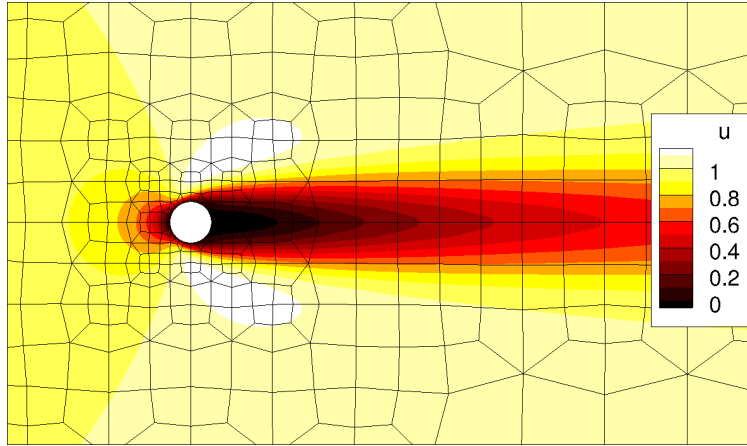


Figure 10: Cylinder test case.

The time-explicit simulations use the Williamson’s low-storage 3rd order Runge-Kutta method [47] as the time-marching scheme, where the time step is dynamically adapted according to the CFL condition. The time-implicit simulations use a BDF1 (backward Euler) scheme where the time-step size is fixed to $\Delta t = 1$ for simplicity. In each case, the linear system (condensed and not) that results from the Newton linearized BDF1+DGSEM discretization is solved using the implementation of the parallel direct sparse solver (PARDISO) that is present in Intel’s Math Kernel Library (MKL).

All simulations are restarted from an $N = 3$ approximation after 10^4 explicit RK3 time steps are taken, which is in turn started from a uniform flow condition. The main reason is that that number of explicit time steps is computationally cheap to compute and that, after those 10^4 time steps, the flow conditions are evolved enough to provide Jacobian matrices that can be reused for multiple solves. If the implicit simulations were started from a uniform flow condition, the Jacobian matrix would have to be computed several times at the beginning of the simulation, which may affect performance. All simulations are time-marched until reaching steady-state, which is assumed when the residual is $\|\tilde{\mathbf{R}}\|_\infty \leq 10^{-9}$.

Figure 11 shows the evolution of the residual as a function of the elapsed CPU-time for the simulations of order $N = 3$, $N = 5$ and $N = 7$. Both subfigures illustrate the same data, but Figure 11(a) is a semi-log plot, where the start of the simulation can be seen in detail, and 11(b) is a log-log plot, which allows one to see the overall performance of the simulation.

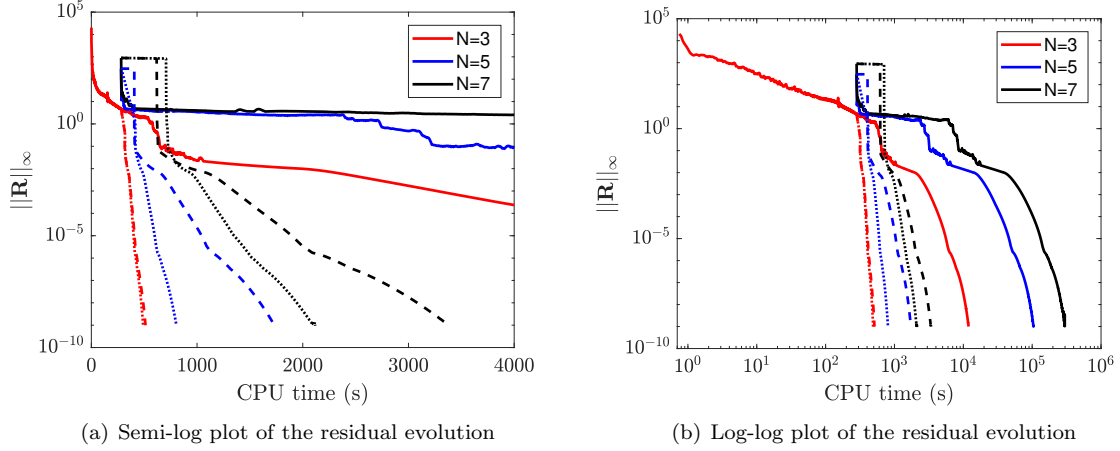


Figure 11: Residual norm vs. CPU-time for the cylinder flow at $Re_\infty = 30$. Solid lines represent the purely explicit simulations (RK3), dashed lines are the implicit simulations solved globally (BDF1), and dotted lines are the implicit simulations solved with the static-condensation method (BDF1+static-condensation).

As can be seen in Figure 11, the convergence rate of the purely explicit simulations is very low, specially at high polynomial orders. In fact, the time-implicit methods outperform them in each case. It is also noteworthy that there is a sudden increase in the residual after the high-order simulations are restarted from the $N = 3$ approximation. This increase is the residual that corresponds to the high-frequency errors of the low-order $N = 3$ approximation.

In the implicit simulations, there is a plateau after the sudden residual increase, which mainly corresponds to the Jacobian factorization times. The Jacobian computation time also adds to the plateau, but it is negligible with respect to the computational cost of the LU decomposition.

There is a small overhead in the statically condensed simulations with respect to the global ones, as can be easily appreciated in the duration of the plateau for the simulations of $N = 7$. This extra computing time is invested in assembling the condensed system, which requires inverting the blocks of $\underline{\mathbf{A}}_{ii}$, performing matrix-matrix multiplications and subtractions for the condensed matrix, and matrix-vector multiplications for the condensed RHS.

The statically condensed simulations are computationally more efficient than their globally solved counterparts. Namely, the extra computational resources that are needed for the condensation operations are rewarded with a faster convergence rate. In other words, the slope of the decrease of the residual norm is steeper for the statically condensed simulations.

Figure 12 shows the performance of the statically condensed and globally solved simulations with respect to the explicit simulations. It can be seen that speed-ups can be achieved with both methods, but that the statically condensed excel when the polynomial order is increased. The speed-up is as high as 140 for $N = 7$ with respect to the traditional explicit method, which is about 50% faster than the implicit method that solves the global system. The change of slope that is observed in the statically condensed speed-ups for high polynomial orders is likely to be caused by the extra operations of the static-condensation method, which in this work are performed with the global sparse matrices. In any case, the convergence rate of the simulations where PARDISO is applied to the statically condensed system, is always higher than the one of simulations where PARDISO is applied to the global system.

A further advantage of using static condensation is that the statically condensed system, besides being smaller in size, is better conditioned than the original global system. This behavior was observed by Sherwin et al [28] for their statically condensable DG method, and is shown in Figure 13 for the system matrices that come from the time-implicit GL-DGSEM discretization of the flow past a cylinder at $Re_\infty = 30$ and $Ma_\infty = 0.2$.

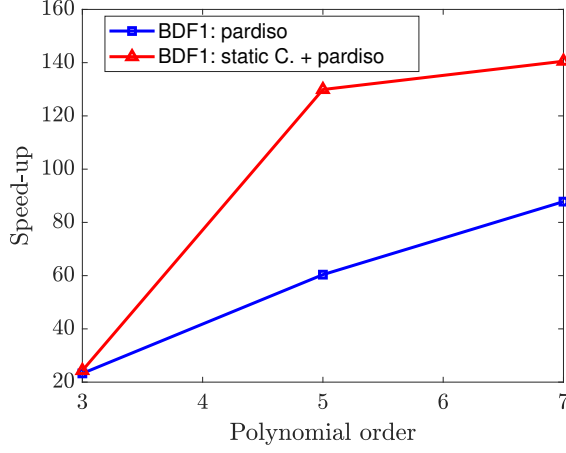


Figure 12: Enhanced performance of the static-condensation method for the cylinder test case.

The L_2 condition number of the Jacobian matrices was determined as the ratio of the largest and smallest eigenvalues, which were estimated using the shift-and-invert algorithm for sparse matrices that is implemented in the ARPACK library [48]. In the example presented here, the maximum eigenvalue of the global and the statically condensed systems are very close. The condition number of the latter is smaller, mainly because the minimum eigenvalue is moved to the left (away from the complex plane origin).

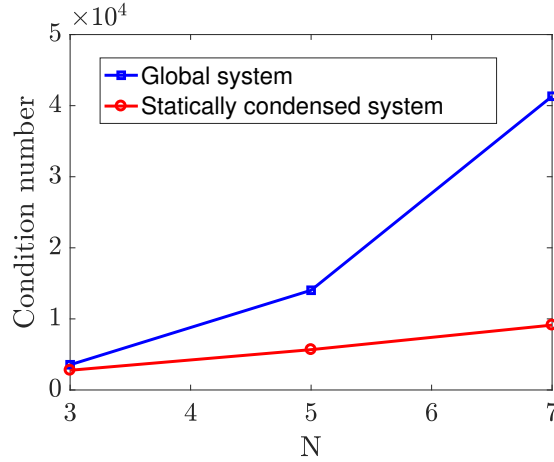


Figure 13: L2 condition number of the system matrix for the global system and the statically condensed one.

The globally solved time-implicit discretizations suffer from an even-odd behavior, which is the reason why no results are reported for even polynomial orders in Figures 11 - 13. The PARDISO solver is not able to converge on the global system for the discretizations of order $N = 4$ and $N = 6$ with the specified settings: $\Delta t = 1$, when the simulations are restarted from the $N = 3$ solution after 10^4 time steps.

The even-odd behavior is not observed in the statically condensed system, which can be solved with PARDISO using the exact setup as for odd N . In fact, the computation times for even polynomial orders fall between the ones obtained for odd polynomial orders, as one would expect. This is remarkable since it means that static condensation provides robustness to the linear problem of the analyzed case and allows

to obtain adequate solutions in otherwise unsolvable cases.

Several strategies were tested to obtain the solution of the non-convergent (globally solved) cases:

1. Modify the PARDISO parameters, such as the number of iterative refinement steps and the pivot perturbation. This yielded no improvement.
2. Restart from a solution of order $N = 4$ after 10^4 time steps (instead of order $N = 3$). This did not work for any of the problematic cases.
3. Restart from a solution of order $N = 4$ after 2×10^4 time steps. This only worked for the $N = 6$ test case.
4. Restart from a solution of order $N = 4$ after 2×10^4 time steps and also reduce the time-step size to $\Delta t = 0.1$. This worked for both $N = 4$ and $N = 6$.

Figure 14 shows the evolution of the residual as a function of the CPU-time for the even polynomial orders, $N = 4$ and $N = 6$. Strategy 4 is retained for $N = 4$ and Strategy 3 is retained for $N = 6$, since that one provides a better performance than Strategy 4. As can be seen, the advantages of using the static-condensation method are more evident for even polynomial orders in this particular test case.

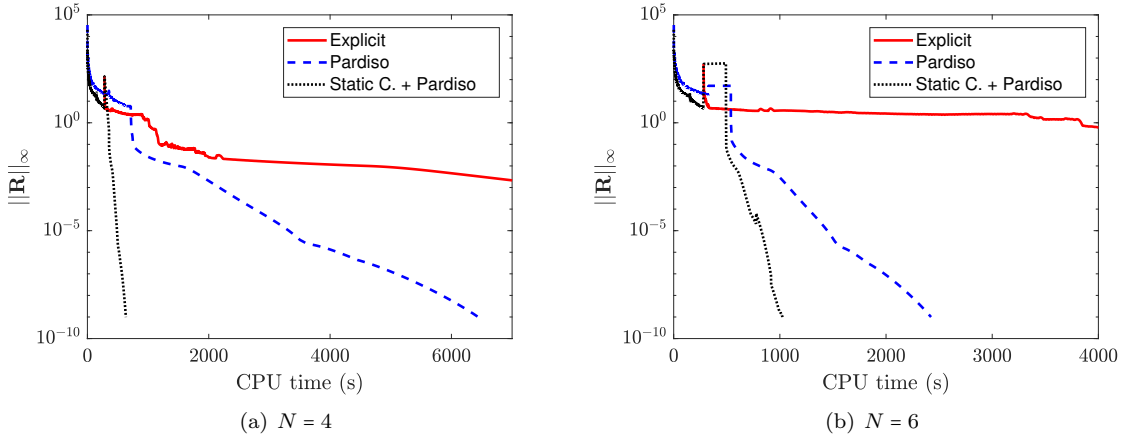


Figure 14: Residual norm vs CPU-time for the cylinder at $Re_\infty = 30$. Even polynomial orders.

The lower condition number of the statically condensed linear systems suggests that the static-condensation method may also improve the convergence rate when using Krylov subspace linear solvers. In fact, the convergence rate of a Krylov subspace method is directly related to the spectrum of the linear operator [49]. We now present a test that supports that idea.

In the cylinder test, the linear system is solved using a GMRES solver with a simple point Jacobi preconditioner. Specifically, the GMRES solver that is implemented in the PETSc library [50] is used. Figure 15 shows the linear system residual as a function of the GMRES iterations for polynomial orders $N = 3$ and $N = 5$. When a time step starts to be solved, a large increase in the linear system residual is exhibited, and every time a new Newton iteration starts there is a small increase in the linear system residual.

As can be seen in Figure 15(a), the $N = 3$ statically condensed simulation takes several time steps while the globally solved one fails to converge the Newton method and reaches the maximum number of iterations allowed before starting the next time step. This behavior is even more pronounced in the $N = 5$ simulation, where the statically condensed simulation advances while the globally solved one diverges.

All in all, although a very simple preconditioner is used (The point Jacobi preconditioner is known to be sub-optimal for high-order methods [51, 52]), the test shows that statically condensing the GL-DGSEM

has a positive impact in the convergence rate when using GMRES for the selected test case. As a matter of fact, the static-condensation operations can be seen as an extra preconditioning technique.

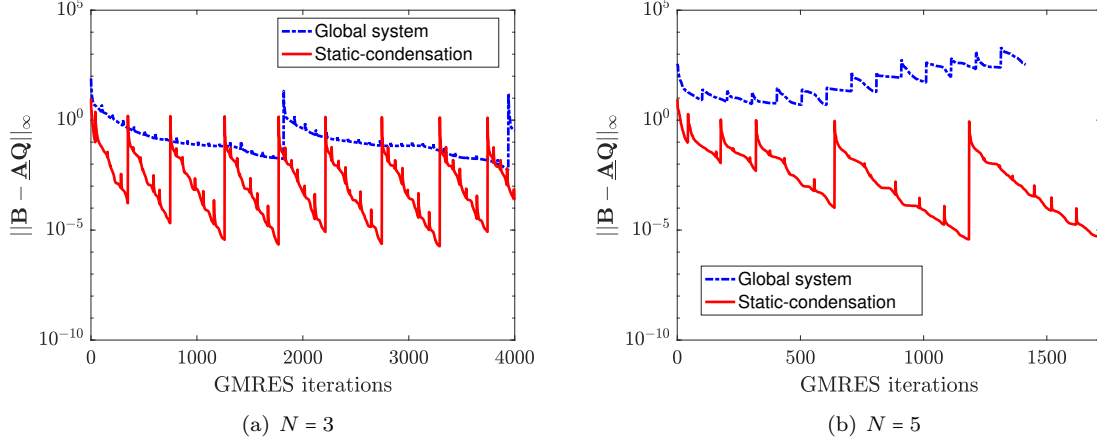


Figure 15: Performance of the static-condensation method with a GMRES solver.

5. Final Remarks

In this paper, we have shown that the DGSEM with Gauss-Lobatto nodes can be directly formulated as a Schur complement problem and solved in an efficient manner using static condensation, where the matrix that needs to be inverted to obtain the Schur complement is block-diagonal. As a result, a statically condensed GL-DGSEM is presented, which does not impose strong constraints on the choice of the basis functions or the form of the numerical fluxes (as other statically condensed DG methods).

It is shown, by means of a numerical example with the compressible Navier-Stokes equations, that static condensation produces speed-ups of up to 140 when compared to the time-explicit GL-DGSEM, and speed-ups of up to 2 when compared with the time-implicit GL-DGSEM that solves the global system directly.

We have shown that the method proposed here does not suffer from a detrimental even-odd behavior, which affects the globally solved system, when solving the subsonic flow past a cylinder. As a result, we can conclude that statically condensing the system provides robustness to the implicit time-discretization of the GL-DGSEM.

In addition, the statically condensed matrices of the presented example are better conditioned than the global matrices they are constructed from, since the minimum eigenvalue is moved away from the origin of the complex plane. This is a likely reason of the improved robustness.

The findings in this paper constitute a further advantage of using GL-DGSEM over G-DGSEM or other variants of the DG method. In summary, GL-DGSEM is computationally cheaper, easier to implement, it enables the formulation of provably stable *uncrashable* schemes (as long as positivity is satisfied in nonlinear problems), allows larger time steps in time-explicit discretizations, enables unified formulations of certain viscous numerical fluxes, and we now prove that it can be used to formulate a statically condensed DG method.

Acknowledgments

This project has received funding from the European Union's Horizon 2020 Research and Innovation Program under the Marie Skłodowska-Curie grant agreement No 675008 for the SSeMID project. This work was supported by a grant from the Simons Foundation (#426393, David Kopriva). Andrés Rueda-Ramírez

would like to thank Prof. Gustaaf Jacobs for his hospitality in San Diego, where part of this work was developed.

The authors acknowledge the computer resources and technical assistance provided by the *Centro de Supercomputación y Visualización de Madrid* (CeSViMa).

References

References

- [1] Z. J. Wang, K. Fidkowski, R. Abgrall, F. Bassi, D. Caraeni, A. Cary, H. Deconinck, R. Hartmann, K. Hillewaert, H. T. Huynh, N. Kroll, G. May, P.-O. Persson, B. van Leer, M. Visbal, B. van Leer, M. Visbal, High-order CFD methods: current status and perspective, *International Journal for Numerical Methods in Fluids* 72 (8) (2013) 811–845. doi:10.1002/flid.3767.
- [2] E. Ferrer, R. H. Willden, A high order Discontinuous Galerkin - Fourier incompressible 3D Navier-Stokes solver with rotating sliding meshes, *Journal of Computational Physics* 231 (21) (2012) 7037–7056. doi:10.1016/j.jcp.2012.04.039. URL <http://dx.doi.org/10.1016/j.jcp.2012.04.039>
- [3] E. Ferrer, An interior penalty stabilised incompressible discontinuous Galerkin–Fourier solver for implicit large eddy simulations, *Journal of Computational Physics* 348 (2017) 754–775. doi:10.1016/j.jcp.2017.07.049.
- [4] A. F. Antoniadis, D. Drikakis, B. Zhong, G. Barakos, R. Steijl, M. Biava, L. Vigeveno, A. Brocklehurst, O. Boelens, M. Dietz, M. Embacher, W. Khier, Assessment of CFD methods against experimental flow measurements for helicopter flows, *Aerospace Science and Technology* 19 (1) (2012) 86–100. doi:10.1016/j.ast.2011.09.003. URL <http://dx.doi.org/10.1016/j.ast.2011.09.003>
- [5] D. Schwamborn, T. Gerhold, R. Heinrich, The dlr tau-code: recent applications in research and industry, *Eccomas* (2006) 1–25.
- [6] L. Cambier, The Onera elsA CFD software: input from research and feedback from industry, *Mechanics & Industry* 14 (2013) (2019) 159–174. doi:10.1051/meca/2013056.
- [7] S. Marras, J. F. Kelly, M. Moragues, A. Müller, M. A. Kopera, M. Vázquez, F. X. Giraldo, G. Houzeaux, O. Jorba, A Review of Element-Based Galerkin Methods for Numerical Weather Prediction: Finite Elements, Spectral Elements, and Discontinuous Galerkin, *Archives of Computational Methods in Engineering* 23 (4) (2016) 673–722. doi:10.1007/s11831-015-9152-1.
- [8] A. Mignone, G. Bodo, S. Massaglia, T. Matsakos, O. Tesileanu, C. Zanni, A. Ferrari, PLUTO: a Numerical Code for Computational Astrophysics, *The Astrophysical Journal Supplement Series* 170 (2007) 228–242. arXiv:0701854, doi:10.1086/513316. URL <http://arxiv.org/abs/astro-ph/0701854> <http://dx.doi.org/10.1086/513316>
- [9] G. L. Bryan, M. L. Norman, B. W. O. Shea, T. Abel, J. H. Wise, M. J. Turk, D. R. Reynolds, D. C. Collins, P. Wang, S. W. Skillman, B. Smith, R. P. Harkness, J. Bordner, J.-h. Kim, M. Kuhlen, H. Xu, N. Goldbaum, ENZO : AN ADAPTIVE MESH REFINEMENT CODE FOR ASTROPHYSICS, *The Astrophysical Journal Supplement Series* 211 (2) (2014) 1–52. doi:10.1088/0067-0049/211/2/19.
- [10] A. D. Beck, D. G. Flad, C. Tonhäuser, G. Gassner, C. D. Munz, On the Influence of Polynomial De-aliasing on Subgrid Scale Models, *Flow, Turbulence and Combustion* 97 (2) (2016) 475–511. doi:10.1007/s10494-016-9704-y.
- [11] G. Gassner, D. A. Kopriva, A Comparison of the Dispersion and Dissipation Errors of Gauss and Gauss–Lobatto Discontinuous Galerkin Spectral Element Methods, *SIAM Journal on Scientific Computing* 33 (5) (2011) 2560–2579. doi:10.1137/100807211. URL <http://epubs.siam.org/doi/10.1137/100807211>
- [12] J. Manzanero, A. M. Rueda-Ramírez, G. Rubio, E. Ferrer, The Bassi Rebay 1 scheme is a special case of the Symmetric Interior Penalty formulation for discontinuous Galerkin discretisations with Gauss–Lobatto points, *Journal of Computational Physics* 363 (2018) 1–10. doi:10.1016/j.jcp.2018.02.035. URL <https://doi.org/10.1016/j.jcp.2018.02.035>
- [13] D. Kopriva, Implementing spectral methods for partial differential equations: Algorithms for scientists and engineers, Springer Science & Business Media, 2009.
- [14] J. Manzanero, G. Rubio, E. Ferrer, E. Valero, D. A. Kopriva, Insights on Aliasing Driven Instabilities for Advection Equations with Application to Gauss–Lobatto Discontinuous Galerkin Methods, *Journal of Scientific Computing* 75 (3) (2018) 1262–1281. arXiv:1705.01503, doi:10.1007/s10915-017-0585-6.
- [15] G. J. Gassner, A. R. Winters, D. A. Kopriva, Split form nodal discontinuous Galerkin schemes with summation-by-parts property for the compressible Euler equations, *Journal of Computational Physics* 327 (2016) 39–66. arXiv:1604.06618, doi:10.1016/j.jcp.2016.09.013.
- [16] A. G. Kravchenko, P. Moin, On the effect of numerical errors in large Eddy simulations of turbulent flows, *Journal of Computational Physics* 131 (2) (1997) 310–322. doi:10.1006/jcph.1996.5597.
- [17] T. C. Fisher, M. H. Carpenter, J. Nordström, N. K. Yamaleev, C. Swanson, Discretely conservative finite-difference formulations for nonlinear conservation laws in split form: Theory and boundary conditions, *Journal of Computational Physics* 234 (1) (2013) 353–375. doi:10.1016/j.jcp.2012.09.026. URL <http://dx.doi.org/10.1016/j.jcp.2012.09.026>

- [18] G. J. Gassner, A Skew-Symmetric Discontinuous Galerkin Spectral Element Discretization and Its Relation to SBP-SAT Finite Difference Methods, *SIAM Journal on Scientific Computing* 35 (3) (2013) A1233–A1253. doi:10.1137/120890144. URL <http://epubs.siam.org/doi/abs/10.1137/120890144>
- [19] M. Böhm, A. R. Winters, G. J. Gassner, D. Derigs, F. Hindenlang, J. Saur, An entropy stable nodal discontinuous Galerkin method for the resistive MHD equations. Part I: Theory and numerical verification, *Journal of Computational Physics* 1 (2018) 1–35. doi:10.1016/j.jcp.2018.06.027. URL <https://doi.org/10.1016/j.jcp.2018.06.027>
- [20] J. Manzanero, G. Rubio, D. A. Kopriva, E. Ferrer, E. Valero, A free-energy stable nodal discontinuous Galerkin approximation with summation-by-parts property for the Cahn-Hilliard equation., *arXiv Numerical Analysis* arXiv:arXiv:1902.08089v1, doi:arXiv:1902.08089v1. URL <http://arxiv.org/abs/1902.08089>
- [21] J. Manzanero, G. Rubio, D. A. Kopriva, E. Ferrer, E. Valero, Entropy-stable discontinuous Galerkin approximation with summation-by-parts property for the incompressible Navier-Stokes equations with variable density and artificial compressibility arXiv:1902.08089. URL <http://arxiv.org/abs/1902.08089>
- [22] A. R. Winters, R. C. Moura, G. Mengaldo, G. J. Gassner, S. Walch, J. Peiro, S. J. Sherwin, A comparative study on polynomial dealiasing and split form discontinuous Galerkin schemes for under-resolved turbulence computations, *Journal of Computational Physics* 372 (2018) 1–21. doi:10.1016/j.jcp.2018.06.016. URL <https://doi.org/10.1016/j.jcp.2018.06.016>
- [23] J. Chan, D. C. D. R. Fernandez, M. H. Carpenter, D. C. Del Rey Fernández, M. H. Carpenter, Efficient entropy stable Gauss collocation methods, *SIAM Journal on Scientific Computing* 41 (5) (2019) A2938–A2966. arXiv:1809.01178. URL <http://arxiv.org/abs/1809.01178>
- [24] R. J. Guyan, Reduction of stiffness and mass matrices, *AIAA journal* 3 (2) (1965) 380.
- [25] B. de Veubeke, Displacement and equilibrium models in the finite element method, *Stress analysis* (1965) chapter—9.
- [26] G. Karniadakis, S. Sherwin, *Spectral/hp element methods for computational fluid dynamics*, Oxford University Press, 2013.
- [27] P. E. J. Vos, S. J. Sherwin, R. M. Kirby, From h to p efficiently: Implementing finite and spectral/hp element methods to achieve optimal performance for low- and high-order discretisations, *Journal of Computational Physics* 229 (13) (2010) 5161–5181. doi:10.1016/j.jcp.2010.03.031. URL <http://dx.doi.org/10.1016/j.jcp.2010.03.031>
- [28] S. J. Sherwin, R. M. Kirby, J. Peiró, R. L. Taylor, O. C. Zienkiewicz, On 2D elliptic discontinuous Galerkin methods, *International Journal for Numerical Methods in Engineering* 65 (5) (2006) 752–784. doi:10.1002/nme.1466.
- [29] J. Carrero, B. Cockburn, D. Schötzau, Hybridized globally divergence-free LDG methods. Part I: The Stokes problem, *Mathematics of Computation* 75 (254) (2005) 533–564. doi:10.1090/s0025-5718-05-01804-1.
- [30] B. Cockburn, J. Gopalakrishnan, R. Lazarov, Unified Hybridization of Discontinuous Galerkin, Mixed, and Continuous Galerkin Methods for Second Order Elliptic Problems, *Society for Industrial and Applied Mathematics* 47 (2) (2009) 1319–1365.
- [31] N. C. Nguyen, J. Peraire, B. Cockburn, An implicit high-order hybridizable discontinuous Galerkin method for nonlinear convection-diffusion equations, *Journal of Computational Physics* 228 (23) (2009) 8841–8855. doi:10.1016/j.jcp.2009.08.030. URL <http://dx.doi.org/10.1016/j.jcp.2009.08.030>
- [32] J. Peraire, N.-C. Nguyen, B. Cockburn, A Hybridizable Discontinuous Galerkin Method for the Compressible Euler and Navier-Stokes Equations, *20th AIAA Computational Fluid Dynamics Conference* (2011) 3228.
- [33] G. J. Gassner, A. R. Winters, F. J. Hindenlang, D. A. Kopriva, The BR1 Scheme is Stable for the Compressible Navier – Stokes Equations, Vol. 77, Springer US, 2018. doi:10.1007/s10915-018-0702-1. URL <https://doi.org/10.1007/s10915-018-0702-1>
- [34] D. N. Arnold, F. Brezzi, B. Cockburn, D. Marini, Unified analysis of discontinuous Galerkin methods for elliptic problems, *SIAM J. Numer. Anal.* 39 (5) (2002) 1749–1779.
- [35] E. F. Toro, *Riemann solvers and numerical methods for fluid dynamics: a practical introduction*, Springer Science & Business Media, 2013.
- [36] J. Douglas, T. Dupont, Interior Penalty Procedures for Elliptic and Parabolic Galerkin Methods, *Computing Methods in Applied Sciences* (2008) 207–216 doi:10.1007/bfb0120591.
- [37] F. Bassi, S. Rebay, G. Mariotti, S. Pedinotti, M. Savini, A high-order accurate discontinuous finite element method for inviscid and viscous turbomachinery flows, in: *Proceedings of the 2nd European Conference on Turbomachinery Fluid Dynamics and Thermodynamics*, Technologisch Instituut, Antwerpen, Belgium, 1997, pp. 99–109.
- [38] F. Bassi, S. Rebay, A high-order accurate discontinuous finite element method for the numerical solution of the compressible Navier-Stokes equations, *Journal of Computational Physics* 131 (1997) 267–279. doi:http://dx.doi.org/10.1006/jcph.1996.5572. URL <http://isn-csm.mit.edu/literature/1997-jcp-bassi.pdf>
- [39] K. Black, A conservative spectral element method for the approximation of compressible fluid flow, *Kybernetika* 35 (1) (1999) 133–146.
- [40] A. M. Rueda-Ramírez, G. Rubio, E. Ferrer, E. Valero, Truncation Error Estimation in the p-Anisotropic Discontinuous Galerkin Spectral Element Method, *Journal of Scientific Computing* 78 (1) (2019) 433–466. doi:10.1007/s10915-018-0772-0.
- [41] A. M. Rueda-Ramírez, J. Manzanero, E. Ferrer, G. Rubio, E. Valero, A p-multigrid strategy with anisotropic p-adaptation

- based on truncation errors for high-order discontinuous Galerkin methods, *Journal of Computational Physics* 378 (2019) 209–233. doi:10.1016/j.jcp.2018.11.009.
- [42] P. Fernandez, N. C. Nguyen, J. Peraire, The hybridized Discontinuous Galerkin method for Implicit Large-Eddy Simulation of transitional turbulent flows, *Journal of Computational Physics* 336 (May) (2017) 308–329. doi:10.1016/j.jcp.2017.02.015.
 - [43] S. Soon, B. Cockburn, H. K. Stolarski, A hybridizable discontinuous Galerkin method for linear elasticity, *International Journal for Numerical Methods in Engineering* 80 (80) (2009) 1058–1092.
 - [44] S. Petersen, C. Farhat, T. Radek, A space–time discontinuous Galerkin method for the solution of the wave equation in the time domain Steffen, *INTERNATIONAL JOURNAL FOR NUMERICAL METHODS IN ENGINEERING* 78 (2009) 275–295.
 - [45] L. S. Blackford, A. Petitet, R. Pozo, K. Remington, R. C. Whaley, J. Demmel, J. Dongarra, I. Duff, S. Hammarling, G. Henry, Others, An updated set of basic linear algebra subprograms (BLAS), *ACM Transactions on Mathematical Software* 28 (2) (2002) 135–151.
 - [46] E. Anderson, Z. Bai, C. Bischof, S. Blackford, J. Demmel, J. Dongarra, J. Du Croz, A. Greenbaum, S. Hammarling, A. McKenney, D. Sorensen, *LAPACK Users' Guide*, 3rd Edition, Society for Industrial and Applied Mathematics, Philadelphia, PA, 1999.
 - [47] J. H. Williamson, Low-storage Runge-Kutta schemes, *Journal of Computational Physics* 35 (1) (1980) 48–56.
 - [48] R. B. Lehoucq, D. C. Sorensen, C. Yang, *ARPACK users' guide: solution of large-scale eigenvalue problems with implicitly restarted Arnoldi methods*, Vol. 6, Siam, 1998.
 - [49] Y. Saad, *Iterative methods for sparse linear systems*, SIAM, 2003.
 - [50] S. Abhyankar, J. Brown, E. M. Constantinescu, D. Ghosh, B. F. Smith, H. Zhang, *PETSc/TS: A Modern Scalable ODE/DAE Solver Library*, arXiv preprint arXiv:1806.01437.
 - [51] E. M. Rønquist, A. T. Patera, Spectral element multigrid. I. Formulation and numerical results, *Journal of Scientific Computing* 2 (4) (1987) 389–406. doi:10.1007/BF01061297.
 - [52] P.-O. Persson, J. Peraire, Newton-GMRES Preconditioning for Discontinuous Galerkin Discretizations of the Navier-Stokes Equations, *SIAM Journal on Scientific Computing* 30 (6) (2008) 2709–2733.